Endocannabinoids Tune Intrinsic Excitability in O-LM Interneurons by Direct Modulation of Postsynaptic Kv7 Channels

Salvatore Incontro, Malika Sammari, Fodil Azzaz, Yanis Inglebert, Norbert Ankri, Michael Russier, Jacques Fantini, Dominique Debanne

Development/Plasticity/Repair

Endocannabinoids Tune Intrinsic Excitability in O-LM Interneurons by Direct Modulation of Postsynaptic Kv7 Channels

Salvatore Incontro, Malika Sammari, Fodil Azzaz, Yanis Inglebert, Norbert Ankri, Michael Russier, Jacques Fantini, and Dominique Debanne

Unité de Neurobiologie des canaux Ioniques et de la Synapse, UMR 1072, Institut National de la Santé et de la Recherche Médicale, Aix-Marseille Université, 13015 Marseille, France

KCNQ-Kv7 channels are found at the axon initial segment of pyramidal neurons, where they control cell firing and membrane potential. In oriens lacunosum moleculare (O-LM) interneurons, these channels are mainly expressed in the dendrites, suggesting a peculiar function of Kv7 channels in these neurons. Here, we show that Kv7 channel activity is upregulated following induction of presynaptic long-term synaptic depression (LTD) in O-LM interneurons from rats of both sex, thus resulting in a synergistic long-term depression of intrinsic excitability (LTD-IE). Both LTD and LTD-IE involve endocannabinoid (eCB) biosynthesis for induction. However, although LTD is dependent on cannabinoid type 1 receptors, LTD-IE is not. Molecular modeling shows a strong interaction of eCBs with Kv7.2/3 channel, suggesting a persistent action of these lipids on Kv7 channel activity. Our data thus unveil a major role for eCB synthesis in triggering both synaptic and intrinsic depression in O-LM interneurons.

Key words: **2-AG; interneurons; intrinsic plasticity; LTD; M-current; synaptic plasticity**

Significance Statement

In principal cells, Kv7 channels are essentially located at the axon initial segment. In contrast, in O-LM interneurons, Kv7 channels are highly expressed in the dendrites, suggesting a singular role of these channels in O-LM cell function. Here, we show that LTD of excitatory inputs in O-LM interneurons is associated with an upregulation of Kv7 channels, thus resulting in a synergistic LTD of LTD-IE. Both forms of plasticity are mediated by the biosynthesis of eCBs. Stimulation of CB1 receptors induces LTD, whereas the direct interaction of eCBs with Kv7 channels induces LTD-IE. Our results thus provide a previously unexpected involvement of eCBs in long-lasting plasticity of intrinsic excitability in GABAergic interneurons.

Introduction

Interneurons are fundamental components of the cortical area, orchestrating the complex machinery that governs brain rhythms. The control of pyramidal cell activity by GABAergic interneurons is required for the execution of hippocampal functions during spatial memory formation. Hippocampal interneurons consist of a diverse population of cell types that have distinct postsynaptic domains and therefore differentially control input/output activity (Pelkey et al., 2017). In the hippocampus, parvalbumin (PV)- and somatostatin (SOM)-expressing interneurons form two broad subtypes of interneurons that preferentially target perisomatic and distal dendritic regions of pyramidal neurons, respectively, and are active on different phases of the theta cycle (Klausberger et al., 2003; Klausberger and Somogyi, 2008; Varga et al., 2012).

Oriens lacunosum moleculare (O-LM) interneurons are SOM positive and selectively active during theta oscillations, gamma oscillations, and fast ripples (Pangalos et al., 2013). They produce feed-back inhibition to pyramidal neurons. Receiving glutamatergic inputs from pyramidal neurons, they not only inhibit the apical dendrites of CA1 pyramidal neurons in the lacunosum moleculare region but they also inhibit interneurons located in the stratum radiatum (Leão et al., 2012). Therefore, they may differentially modulate glutamatergic inputs from CA3 neurons and from entorhinal cortex, respectively, via the control of

Received June 21, 2021; revised Aug. 24, 2021; accepted Sep. 24, 2021.

Author contributions: S.I. and D.D. designed research; S.I., M.S., F.A., Y.I., and J.F. performed research; Y.I., N.A., and M.R. contributed unpublished reagents/analytic tools; S.I., M.S., F.A., N.A., and D.D. analyzed data; and S.I. and D.D. wrote the paper.

This work was supported by the Institut National de la Santé et de la Recherche Médicale, Aix-Marseille Université, NeuroMarseille, and the Fondation pour la Recherche Médicale (FRM DEQ20180839583 to D.D.). We thank Dr. J.J. Ramirez-Franco for help with use of the confocal microscope and Drs. P Delmas, JP Mothet, R Nicoll, and G Sandoz for reading a preliminary version of the manuscript.

The authors declare no competing financial interests.

Correspondence should be addressed to Salvatore Incontro at salvincontro@gmail.com or Dominique Debanne at dominique.debanne@inserm.fr.

https://doi.org/10.1523/JNEUROSCI.1279-21.2021

inhibition of the dendritic region, where Schaffer collaterals project, or via direct inhibition of the dendritic region, where temporoammonic pathways project. They receive glutamatergic inputs from CA1 pyramidal neurons and cholinergic inputs from the medial septum (Leão et al., 2012). O-LM interneurons express a wide range of voltage-gated channels including Kv7.2/3 channels in the dendrites of the O-LMs (Lawrence et al., 2006).

KCNQ-Kv7 potassium channels are found at the axon initial segment (AIS) of pyramidal neurons, where they control cell firing and resting membrane potential (Shah et al., 2008). Kv7 channels oppose depolarization by creating a noninactivating outward current. These channels are inhibited by stimulating many receptors including muscarinic receptors (Delmas and Brown, 2005). On the other hand, they are activated by somatostatin and by endocannabinoids (eCBs; Larsson et al., 2020). Although redistribution of these channels along the AIS has been demonstrated in homeostatic plasticity (Kuba et al., 2015), the contribution of Kv7 channels to functional plasticity is still unclear.

Classically, activity-dependent plasticity of inhibitory circuits is thought to be achieved by regulation of excitatory synaptic drive to inhibitory interneurons (McMahon and Kauer, 1997; Alle et al., 2001; Perez et al., 2001; Kullmann and Lamsa, 2007; Lamsa et al., 2007; Pelletier and Lacaille, 2008; Kullmann et al., 2012; Péterfi et al., 2012; Vasuta et al., 2015) or by plasticity of inhibitory synaptic transmission on pyramidal neurons (Vickers et al., 2018; Udakis et al., 2020). However, functional plasticity might also be achieved through the regulation of voltage-gated ion channels that control synaptic integration and spike initiation (Titley et al., 2017; Debanne et al., 2019). PV interneurons express long-lasting intrinsic plasticity following induction of long-term synaptic potentiation (LTP) or activity deprivation (Campanac et al., 2013; Gainey et al., 2018). SOM interneurons have been shown to express intrinsic plasticity following learning (McKay et al., 2013). However, this study was based on a comparison of interneurons recorded in different animals that experienced different conditioning, and it is still not known whether single SOM interneurons as O-LM cells express intrinsic plasticity.

In hippocampal neurons, synaptic and intrinsic plasticity are expressed in parallel (Debanne et al., 2019). This synergy is functionally important as both forms of plasticity act in concert to either promote or reduce excitation. However, the molecular mechanisms linking the two forms of plasticity are still unclear. Here, we show that long-term synaptic depression (LTD) and LTD of intrinsic excitability (LTD-IE) of neurons expressed in O-LM interneurons are both mediated by lipid biosynthesis. Stimulation of cannabinoid type 1 (CB1) receptors induces LTD, whereas the direct interaction of eCBs with Kv7.2/3 channels induces LTD-IE. Our results thus provide a previously unexpected involvement of eCBs in long-lasting plasticity of intrinsic excitability in GABAergic interneurons.

Materials and Methods

Slice preparation. All experiments were conducted according to the European and institutional guidelines for the care and use of laboratory animals (Council Directive 86/609/EEC and French National Research Council) and approved by the local health authority (Préfecture des Bouches-du-Rhône, Marseille). In this study, we used Wistar rats (Charles River Laboratories) of either sex.

Hippocampal slices (350 mm) were prepared from postnatal day (P) 14–21 Wistar rats of both sex. Rats were deeply anesthetized with isoflurane and killed by decapitation. Slices were cut with a vibratome (Leica VT-1200S) in a *N*-methyl-D-glucamine (NMDG) solution containing the following (in mM): 92 NMDG, 1.2 NaH_2PO_4, 30 $NaHCO_3$, 20 HEPES, 25 D-glucose, 5 sodium ascorbate, 2 thiourea, 3 sodium pyruvate, 10 $MgCl_2$, and 0.5 $CaCl_2$. The slices were maintained for 1 h at room temperature in oxygenated (95% O_2/5% CO_2) artificial cerebrospinal fluid (ACSF) containing the following (in mM): 125 NaCl, 2.5 KCl, 0.8 NaH_2PO_4, 26 $NaHCO_3$, 3 $CaCl_2$, 2 $MgCl_2$, 10 D-Glucose.

Electrophysiology. Each slice was transferred to a temperature-controlled (31°C) recording chamber with oxygenated ACSF. O-LM hippocampal interneurons were identified by the location of the soma (stratum oriens of the CA1), morphology (a spindle-shaped cell body horizontally oriented along the pyramidal layer), and the peculiar electrophysiological signature (the characteristic sag depolarizing potential in response to hyperpolarization currents injections and the typical sawtooth shape of action-potential afterhyperpolarizations). In all recordings $GABA_A$ receptors were blocked by picrotoxin (PiTx; 100 μM), and CA3 area was surgically removed to prevent epileptiform bursting. Whole-cell patch-clamp recordings were obtained from CA1 O-LM interneurons. The electrodes were filled with an internal solution containing the following (in mM): 120 K-gluconate, 20 KCl, 10 HEPES, 0 EGTA, $MgCl_26H_2O$, 2 Na_2ATP, 0.1 spermine. Stimulating pipettes filled with extracellular saline were placed in the stratum oriens near the alveus to stimulate inputs coming from the pyramidal neurons.

In control and test conditions, the following parameters were measured in current-clamp mode for 15 min before and at least 15 min after LTD protocol. Apparent input resistance was tested by current injection (−120 pA, 800 ms). EPSPs were evoked at 0.1 Hz, and the stimulus intensity (100 μs, 40–100 μA) was adjusted to evoke subthreshold EPSPs (4–10 mV). Short current injections (70–120 pA, 100 ms) were applied at each sweep to measure the intrinsic excitability as the number of spikes over time. Series resistance was monitored throughout the recording, and only experiments with stable resistance were kept (changes <10%). O-LM cells were held at approximately −65 mV during the experiments before and after the pairing protocol. Liquid junction potential (−12 mV) was not corrected. Before and after LTD induction, a protocol was designed to plot input-output curves by measuring the action potentials (APs) number in response to incrementing steps of current pulses.

To measure the M-current mediated by somato-dendritic Kv7 channels, a voltage-clamp protocol was used consisting in voltage steps from −30 mV to −50 mV (Lawrence et al., 2006). The relaxing component of the M-current was then measured before and after LTD-IE induction.

Induction of LTD and LTD-IE. LTD and LTD-IE were induced in O-LM interneurons with a protocol consisting of 600 pairings between a postsynaptic action potential followed by a presynaptic stimulation of the pyramidal neurons with a delay of 10 ms. These pairings were evoked at a frequency of 5, 10, or 20 Hz in blocks of six with an interblock interval of 10 s at a membrane potential between −50 and −58 mV (Péterfi et al., 2012). For each cell we used a protocol, which allowed us to measure EPSPs, input resistance, and IE, 15 min before and at least 15 min after the LTD protocol.

Data acquisition and analysis. Recordings were obtained using a MultiClamp 700B (Molecular Devices) amplifier and pClamp10 software. Data were sampled at 10 kHz, filtered at 3 kHz, and digitized by a Digidata 1322A Digitizer (Molecular Devices). All data analyses were performed with custom-written software in Igor Pro 6 (WaveMetrics). Input resistance was determined by the subtraction of the steady-state voltage change during hyperpolarizing current injection from the baseline.

Pharmacology. Drugs were all bath applied. PiTx was purchased from Sigma-Aldrich; ZD-7288 [4-(N-ethyl-N-phenylamino)−1,2-dimethyl-6-(methylamino) pyrimidinium chloride], tetrahydrolipstatin (THL), and 2 Arachidonylglycerol (2-AG), JZL-184, AM 251 [*N*-(Piperidin-1-yl)−5-(4-iodophenyl)−1-(2,4-dichlorophenyl)−4-methyl-1*H*-pyrazole-3-carboxamide] from Tocris Bioscience; and N-arachidonoyl-L-serine (ARA-S) from Cayman Chem.

Biocytin filling and confocal microscopy. The dendritic and axonal morphology of the recorded neurons was revealed by biocytin staining. For this, biocytin (0.2–0.4%, Sigma-Aldrich) was added to the pipette solution, and O-LM cells were filled at least 20 min. Biocytin was revealed

with streptavidin complex coupled to Alexa Fluor 488 (Thermo Fisher Scientific), and examined using confocal microscopy (Zeiss, LSM 780). The morphology of the neurons was reconstructed using ImageJ.

Molecular modeling. The 3D structure of the rat Kv7.2 channel has been obtained by homology with the human KCNQ2 protein in apo state (Li et al., 2021). The amino acid sequence of rat Kv7.2 (96.61% sequence homology) was retrieved from UniProtKB-O88943 (KCNQ2_RAT) and submitted to the SWISS-MODEL Interactive Workspace (https://swissmodel.expasy.org/repository/uniprot/O88943). The model is stored in the SWISS-MODEL database (project KCNQ2_RAT O88943 Potassium voltage-gated channel subfamily KQT member 2).

Docking of ara-S and 2-AG on Kv7.2 was performed with HyperChem as previously described (Flores et al., 2019). Energy minimization of each system was performed with the Polak-Ribière conjugate gradient algorithm, with the BIO+ CHARMM force field in Hyperchem 8.0, using a maximum of 3×105 steps, and a root-mean-square (RMS) gradient of 0.01 kcal.Å^{-1}.mol^{-1} was the convergence condition. The energies of interaction were calculated by the ligand energy inspector function of the Molegro Molecular viewer (Molexus IVS, http://molexus.io/molegro-molecular-viewer/).

Microtensiometry. The interaction of 2-AG with synthetic transmembrane (TM) domains derived from the structure of Kv7.2 was studied with a microtensiometer. Synthetic peptides LASFLVYLAEKGE (P1) RSLRFLQILRMI (P2) with a purity >98% were purchased from GeneCust. A monolayer of these synthetic peptides (alone or in combination) was prepared at the air–water interface, and 2-AG was injected in the aqueous subphase. Changes in surface pressure were measured in real time with a Kibron microtensiometer as previously described (Fantini et al., 2016). Control experiments without peptide or with ganglioside monolayers were performed in parallel to ensure the specificity of the results obtained.

Statistics. Pooled data are presented as means ± SEM. Averages were normalized on the five last data points in control (i.e., last 5 min). Statistical comparisons were made using Mann–Whitney or Wilcoxon tests with Prism (GraphPad) software. Differences were considered significant at $p < 0.05$ ($^*p < 0.05$, $^{**}p < 0.01$, $^{***}p < 0.001$).

Results

Coinduction of long-term synaptic and intrinsic depression in O-LM cells

Whole-cell recordings from CA1 O-LM interneurons were obtained in hippocampal slices from P14–P21 rats. O-LM cells were identified in the stratum oriens by the typical electrophysiological behavior (regular spiking discharge with deep afterhyperpolarization and the presence of depolarizing sag on hyperpolarizing current injection (Gastrein et al., 2011) of the cells and the characteristic axonal projection in the lacunosum moleculare (Fig. 1*A*). All experiments were performed in the presence of the GABA receptor antagonist PiTx (100 μM). The cells were held at −65 mV with negative holding current (−10 to −40 pA). EPSPs were evoked by stimulation of the axons of pyramidal neurons in the alveus-oriens region, and excitability was monitored before and after pairing over a period of >40 min (Fig. 1*B*). LTD was induced by pairing single action potentials triggered in the O-LM cell followed 10 ms later by presynaptic stimulation. This was repeated in groups of six at 10 Hz (Péterfi et al., 2012). As already shown in mouse O-LM interneurons (Péterfi et al., 2012), a nearly 50% decrease in the EPSP slope was observed after such negative pairing (NP) protocol (52 ± 3% of the control EPSP slope, $n = 16$; Fig. 1*C*). An increase in the paired-pulse ratio was observed after induction of LTD (from 1.56 ± 0.18 to 2.83 ± 0.27, $n = 5$; Wilcoxon test, $p < 0.05$; Fig. 1*D*), indicating that it is expressed by a presynaptic reduction in glutamate release.

Interestingly, the number of action potentials evoked by moderate current injections (90–120 pA, 100 ms) was significantly reduced after negative pairing (69 ± 6% of control AP number, $n = 16$; Fig. 1*E*). Importantly, no change in input resistance tested with hyperpolarizing pulses was observed (100 ± 3%, $n = 16$; Fig. 1*F*). Input-output curves drawn before and after pairing revealed a marked reduction in intrinsic excitability (Fig. 2*A*). The holding current remained unchanged (−27.3 ± 4.7 pA before and −24.5 ± 4.9 pA after, Wilcoxon, $p > 0.05$). The rheobase (i.e., the minimal current eliciting an action potential) was found to be elevated (from 40 ± 6 pA to 67 ± 9 pA, $n = 16$, Wilcoxon, $p < 0.01$; Fig. 2*B*). Intriguingly, the reduction in excitability was associated with a reduction of the input resistance tested with subthreshold depolarizing pulses (from 473.9 ± 41.5 MΩ to 275.8 ± 37.1 MΩ, $n = 15$; Wilcoxon test, $p < 0.001$; Fig. 2*C*), indicating the involvement of a voltage-dependent conductance activated by depolarizing potentials. This depression of intrinsic excitability could be followed up to 30 min (Fig. 2*D*), indicating that it is long lasting. Thus, negative pairing in O-LM interneurons leads to the coinduction of LTD and LTD-IE. LTD and LTD-IE were found to be linearly related (Fig. 2*E*), suggesting a common induction mechanism.

Induction mechanisms of LTD-IE in O-LM interneurons

As LTD and LTD-IE are induced by negatively pairing postsynaptic APs with EPSPs delayed by 10 ms at a frequency of 10 Hz, we checked the associative nature of the stimulation as well as the frequency dependence.

Postsynaptic spiking alone delivered at 10 Hz was unable to induce either LTD (101 ± 3% of control EPSP slope, $n = 8$) or LTD-IE (93 ± 4% of the control AP number, $n = 8$; Fig. 3*A–C*), whereas in a large fraction of the same neurons, a second episode of postpairing/prepairing induced both LTD (67 ± 8%, $n = 6$) and LTD-IE (70 ± 5%, $n = 6$; Fig. 3*A–C*). Similarly, presynaptic stimulation alone delivered at 10 Hz was unable to induce either LTD (106 ± 7%, $n = 11$) or LTD-IE (98 ± 6%, $n = 11$), whereas in a large fraction of the same neurons a second episode of postpairing/prepairing induced both LTD (71 ± 8%, $n = 9$) and LTD-IE (71 ± 8%, $n = 9$; Fig. 3*D*,*E*). These results show that LTD and LTD-IE induction in O-LM interneurons depends on the association between postsynaptic spiking and presynaptic stimulation.

In a second step, we varied the stimulation frequency during pairing. At 5 Hz, no significant LTD (73 ± 11%, $n = 10$, Wilcoxon, $p > 0.1$) nor LTD-IE (98 ± 8%, $n = 10$, Wilcoxon, $p > 0.1$) was induced (Fig. 4*A*,*B*,*D*). Similarly, no LTD (89 ± 16%, $n = 7$; Wilcoxon, $p > 0.1$) and a very small LTD-IE (81 ± 6, $n = 7$; Wilcoxon, $p < 0.01$) could be induced by stimulation at 20 Hz (Fig. 4*A*,*C*,*E*). Thus, we conclude that LTD and LTD-IE are preferentially induced by stimulation at a frequency of 10 Hz.

LTD-IE in O-LM interneurons is mediated with Kv7 channels

We next focused on the expression mechanism of LTD-IE expressed in O-LM interneurons. As an increase in the rheobase was observed after LTD-IE induction, we first checked whether the voltage threshold of the AP was modulated after negative pairing. However, no difference in the AP threshold was observed before and after induction of LTD-IE (−43.3 ± 1.4 mV in control vs −42.4 ± 1.2 mV; Wilcoxon, $p > 0.1$; Fig. 5*A*). This result thus excludes a change in Nav or Kv1 channels controlling the spike threshold. Moreover, no change in input resistance measured by long hyperpolarizing steps of current was observed, thus excluding a major role of hyperpolarization-activated nucleotide-gated cation (HCN) channels in LTD-IE expression.

As O-LM interneurons express a high density of Kv7 channels in dendrites (Lawrence et al., 2006), we next focused on the

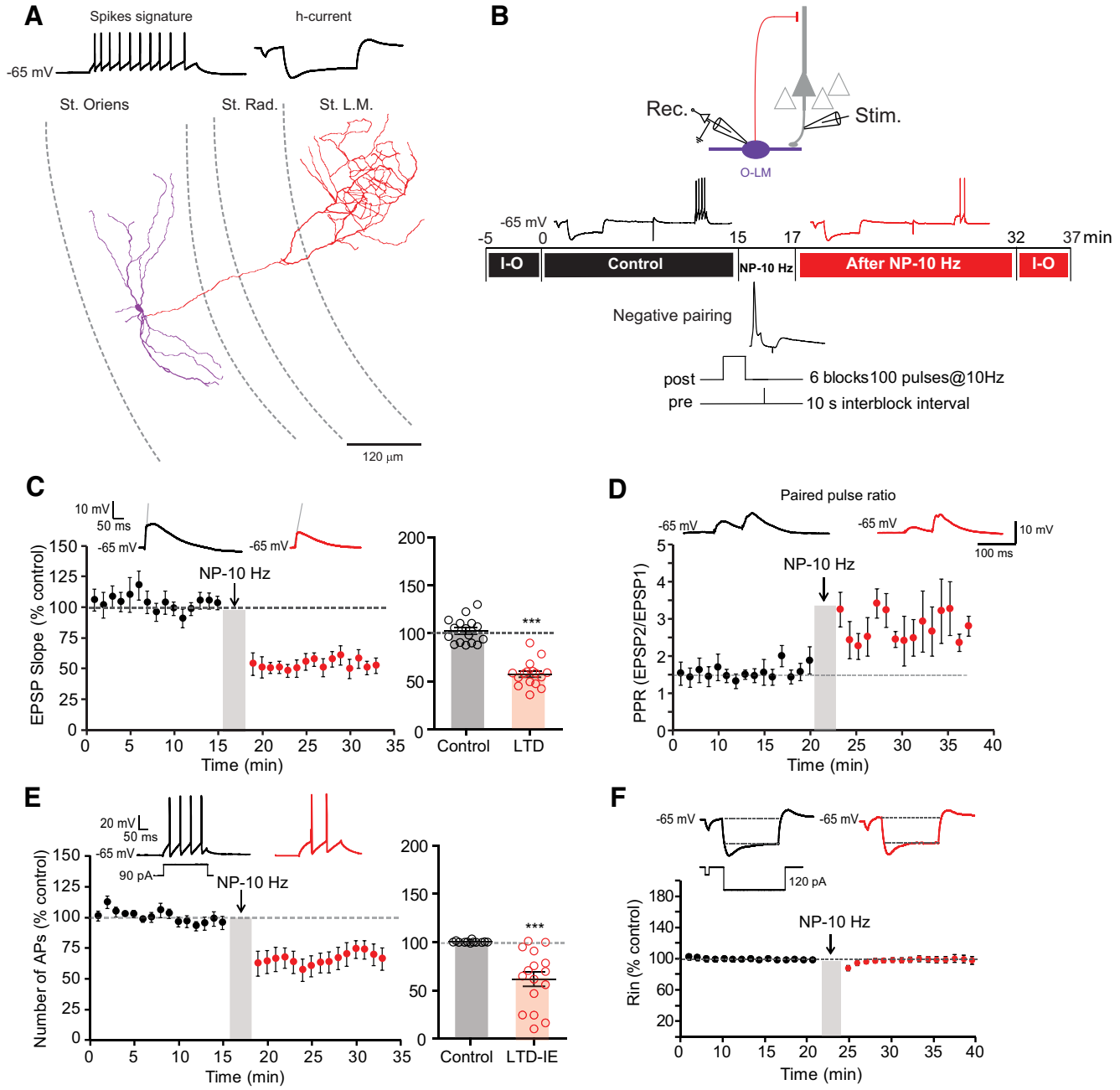

Figure 1. Negative pairing at 10 Hz induces LTD and LTD-IE in O-LM interneurons. ***A***, Morphologic and electrophysiological identification of O-LM interneurons. Reconstruction of an O-LM interneuron. Purple segments represent dendrites, and red segments represent axon. ***B***, Top, Recording and stimulation configuration. Middle, Synaptic transmission and intrinsic excitability is monitored at least 15 min before and after negative pairing delivered at 10 Hz (NP-10 Hz). Input-output (I-O) curves are plotted before and after the two test periods. Bottom, Induction protocol. ***C***, LTD induction by negative pairing. Left, Time course. Right, Pooled data. Wilcoxon test, $^{***}p < 0.001$. ***D***, LTD in O-LM interneurons is associated with an increased paired-pulse ratio. ***E***, Induction of LTD-IE by negative pairing. Left, Time course. Right, Pooled data. Wilcoxon test, $p < 0.001$. ***F***, Lack of input resistance change after negative pairing. Top, Representative traces. Bottom, Time course of normalized input resistance.

Kv7-mediated M-type current. As HCN and Kv7 may have overlapping deactivation and activation profiles, we first measured LTD and LTD-IE in the presence of the specific blocker of HCN channels, ZD-7288 (1 μM; Fig. 5*B–D*). To measure the M-current, O-LM neurons were recorded in voltage clamp at a membrane potential of −30 mV, and negative pulses to −50 mV were applied to measure the deactivation of M-current. Interestingly, the magnitude of the M-current deactivation was significantly increased following induction of LTD-IE (from 26.8 ± 7 pA to 54.2 ± 11.4 pA, $n = 14$; Fig. 6*A*,*B*). Furthermore, the holding current at −30 mV increased from 114.7 ± 27.2 pA to 196.6 ± 27.6 pA ($n = 14$; Fig. 6*B*). To confirm that M-current was effectively measured, the specific antagonist of Kv7 channels, XE-991 (1 μM), was applied at the end of the recording in a few experiments. Most of the current was shown to be blocked in the presence of XE-991 (remaining current, 19.7 ± 4.9 pA, $n = 8$).

Because M-current is upregulated, we next checked whether LTD-IE was specifically blocked in the presence of XE-991. As expected, LTD-IE (97 ± 6%, $n = 9$) but not LTD (49 ± 10%, $n = 9$) was found to be blocked in the presence of 1 μM XE-991 (Fig. 6*C–E*). In addition, no difference in the rheobase nor in the gain was observed on the input-output curves (Fig. 6*F*). Altogether,

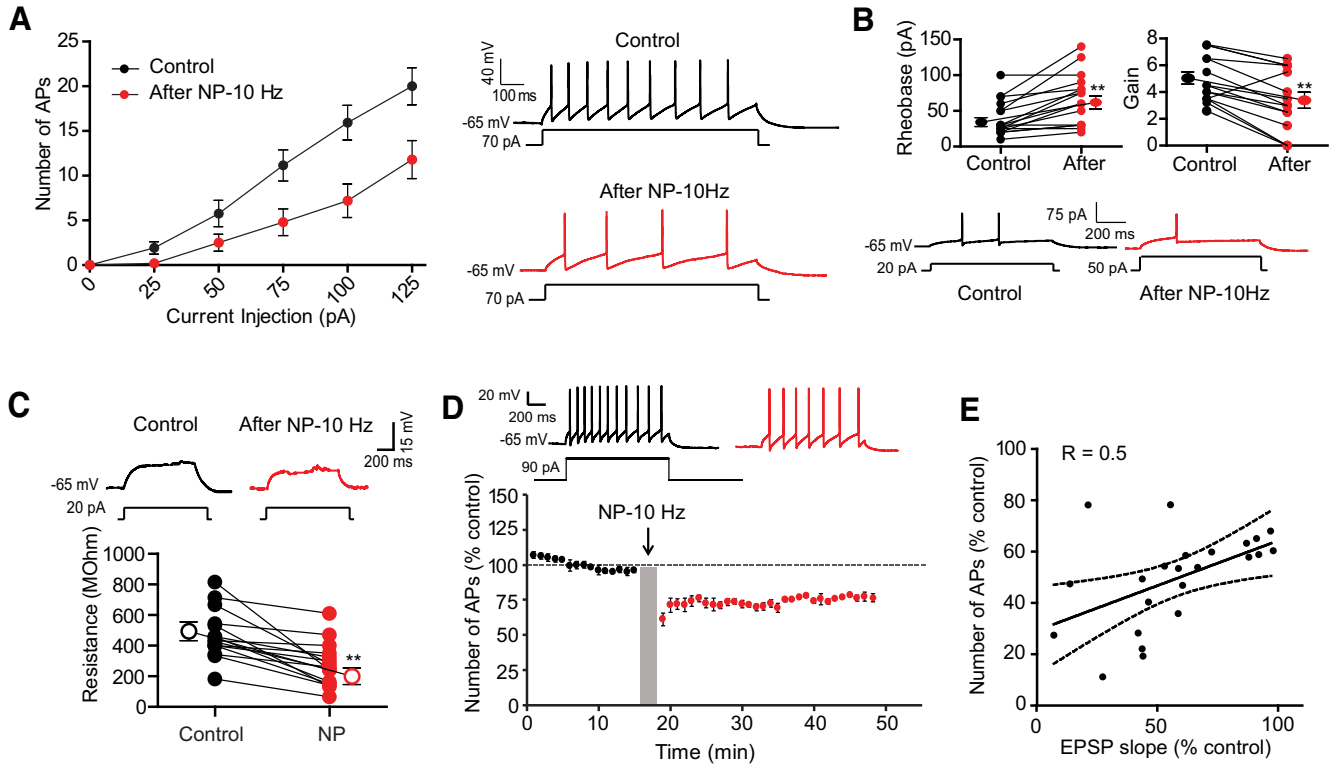

Figure 2. Negative pairing at 10 Hz induces a decrease in input-output curves, rheobase, and input resistance at subthreshold depolarizing currents. ***A***, Input-output curves before and after negative pairing. ***B***, Rheobase is elevated, whereas gain is reduced. $^{**}p < 0.01$. Example of the rheobase increase (here, from 20 pA to 50 pA) after negative pairing. ***C***, Negative paring reduces input resistance tested with subthreshold depolarizing pulses. Top, Representative traces. Bottom, Pooled data. Wilcoxon test, $^{***}p < 0.001$. ***D***, Long-lasting reduction in intrinsic excitability. The reduction in excitability can be followed during >30 min. ***E***, Correlation between normalized AP number and normalized EPSP slope.

these results show that Kv7 channels in O-LM interneurons are upregulated following induction of LTD by negative pairing induced at theta frequency.

eCB synthesis mediates both LTD and LTD-IE in O-LM interneurons

Induction of LTD in O-LM interneurons depends on stimulation of the eCB receptor CB1 (Péterfi et al., 2012). We first checked whether LTD and LTD-IE were both mediated by CB1 receptors. In the presence of the selective antagonist of CB1 receptor, AM-251 (2 μM), no LTD was induced (95 ± 6%, $n = 11$; Wilcoxon, $p > 0.1$), but LTD-IE was virtually unchanged (82 ± 5%, $n = 11$; Fig. 7*A–C*). Furthermore, the rheobase was significantly elevated following negative pairing (from 34.0 ± 5.0 pA to 71.0 ± 12.4 pA, $n = 11$; Wilcoxon, $p < 0.01$; Fig. 7*D*). These results suggest that CB1 receptors mediate LTD of synaptic excitation in O-LM interneurons via a presynaptic modulation of glutamate release but that LTD-IE does not depend on CB1.

Kv7 channels expressed in oocytes are upregulated by eCBs (Larsson et al., 2020). As, Kv7 channels are involved in LTD-IE, we therefore tested whether inhibiting eCB synthesis prevented LTD-IE. As 2-AG is an eCB synthesized by diacylglycerol (DAG) lipase, we therefore tested whether the inhibitor of DAG lipase, THL (also called orlistat), blocked induction of LTD-IE. Application of THL (10 μM) for at least 20 min was found to slightly increase O-LM excitability (Fig. 8*A*). In fact, the rheobase was significantly diminished in the presence of THL (44.6 ± 4.5 pA, $n = 12$ in control solution vs 24.6 ± 4.1 pA, $n = 12$ in THL), suggesting that basal synthesis of 2-AG is sufficient to reduce excitability in O-LM cells. But most important, both LTD and LTD-IE were found to be prevented by inhibiting 2-AG synthesis with THL (Fig. 8*B–D*). In fact, no synaptic modification (99 ± 4% of the control EPSP, $n = 12$) nor excitability change (100 ± 3% of the control AP number, $n = 12$) was observed after negative pairing in THL. In addition, no change in the rheobase was observed after negative pairing in THL (Fig. 8*E*). Thus, these results indicate that 2-AG could be a major effector of both synaptic and intrinsic changes in O-LM interneurons.

As inhibition of eCB synthesis increased excitability, we next verified that application of eCBs reduced intrinsic neuronal excitability in O-LM interneurons. As expected, application of 2-AG (30 μM) reduced O-LM excitability (rheobase in control, 31.4 ± 2.6 pA, $n = 7$; rheobase in 2-AG, 45.7 ± 4.3 pA, $n = 7$; Wilcoxon, $p < 0.05$; Fig. 9*A*). This reduced excitability was associated with a reduction of the input resistance tested with subthreshold depolarizing pulses (2-AG, from 500 ± 49.2 MΩ to 314.5 ± 23.9 MΩ, $n = 7$; Wilcoxon test, $p < 0.05$; Fig. 9*B*). To directly confirm this result, we measured the M-current in voltage clamp applying pulses of membrane potential from −20 mV to −45 mV to measure the deactivation of M-current. Importantly, the magnitude of the M-current was significantly increased following 20 min of 2-AG application (from 63.82 ± 15 pA to 81.13 ± 14.3 pA, $n = 7$; Fig. 9*C*; Wilcoxon test, $p < 0.05$). In the presence of 2-AG, LTD-IE was occluded (Fig. 9*D*,*E*), and no change in rheobase was observed (rheobase in 2-AG, 45.7 ± 4.2 pA, $n = 7$; rheobase in 2-AG after NP, 58.5 ± 3.4 pA, $n = 7$; Wilcoxon, $p > 0.05$; Fig. 9*F*).

Similarly, JZL-184, an inhibitor of the monoacylglycerol lipase, that leads to elevation of 2-AG levels, also reduced excitability through an elevation of the rheobase (from 35.0 ± 4.7 pA, $n =$ 12–47.5 ± 5.2 pA; Wilcoxon, $p < 0.01$; Fig. 10*A*). Furthermore, application of ARA-S, a potent activator of Kv7 channels found in

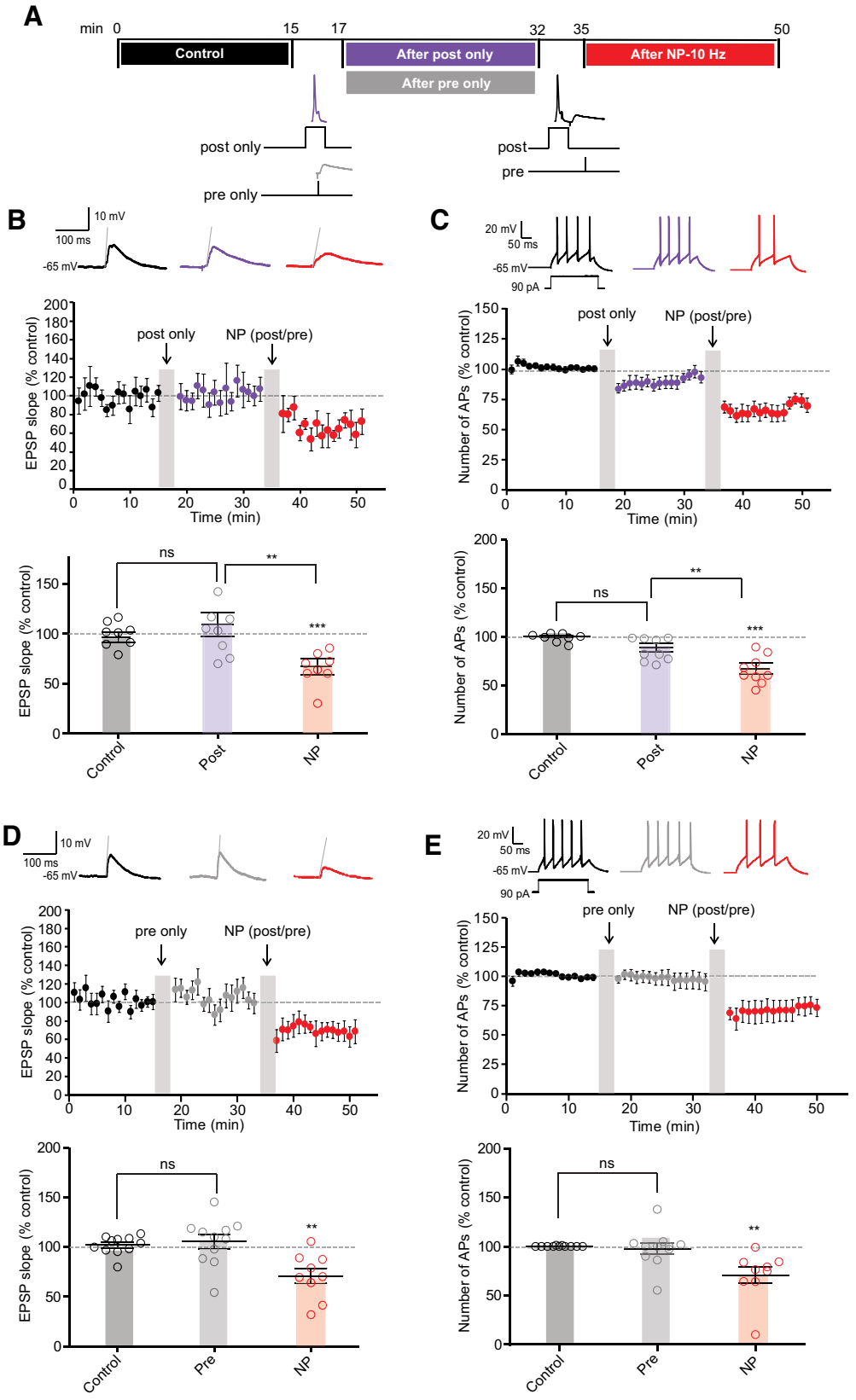

Figure 3. Poststimulation and prestimulation are required for induction of both LTD and LTD-IE. ***A***, Induction protocols. In a first step, the effects of postsynaptic or presynaptic activity (postsynaptic only or presynaptic only) are tested. Then, in each case, postprotocol and pre-protocol delivered at 10 Hz are applied. ***B***, ***C***, Postsynaptic spiking activity results in no synaptic or intrinsic changes, whereas postpairing/prepairing in the same neurons induced LTD and LTD-IE. ***D***, ***E***, Presynaptic activity alone does not change synaptic transmission nor intrinsic excitability, whereas postpairing/prepairing is sufficient to induce LTD and LTD-IE in the same neurons.

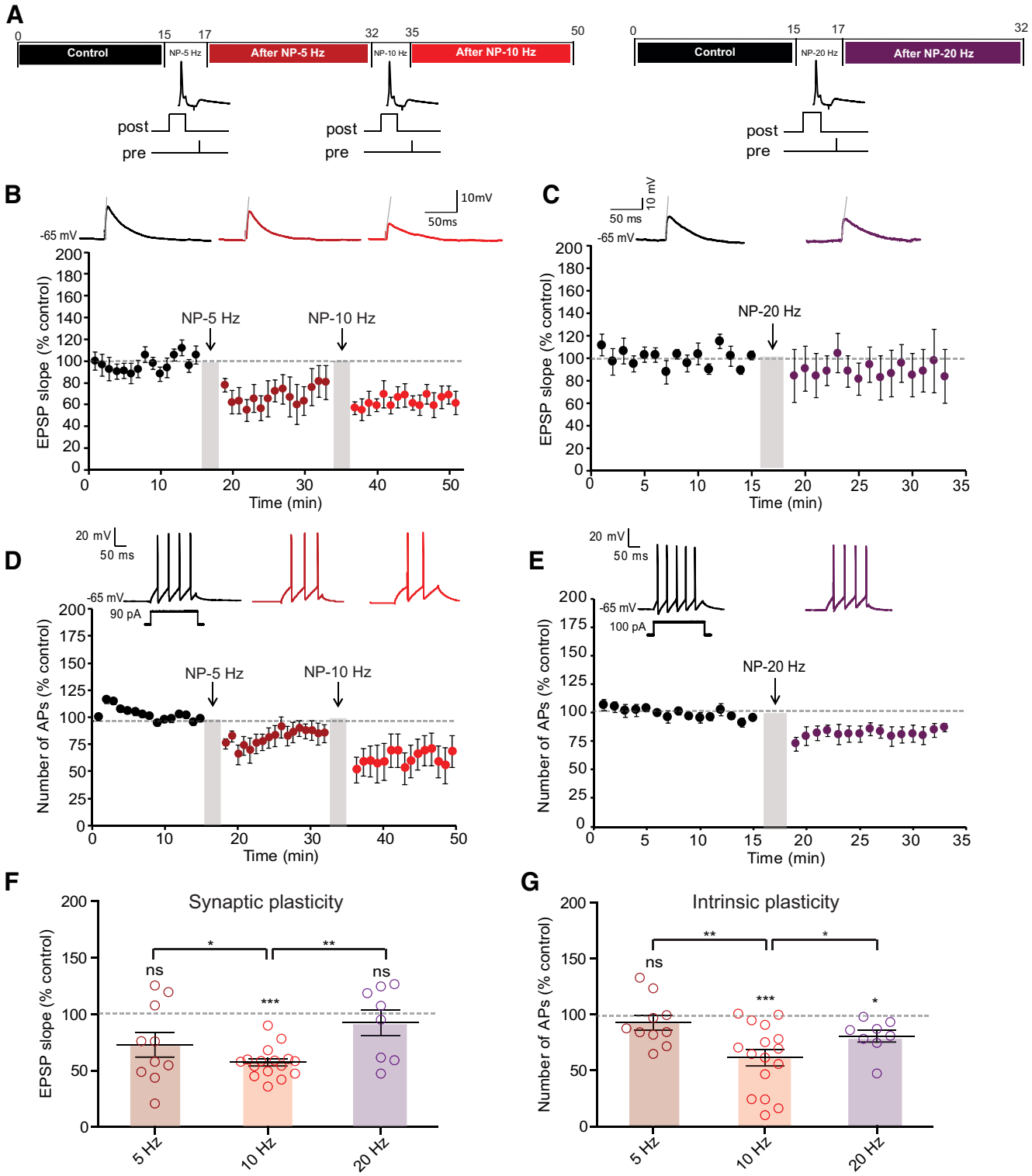

Figure 4. LTD-IE is induced by stimulation at 10 Hz. ***A***, Experimental protocols. Left, Negative pairing at 5 Hz is followed by negative pairing at 10 Hz. Right, Negative pairing at 20 Hz. ***B***, Synaptic changes after negative pairing at 5 Hz and 10 Hz. ***C***, Synaptic changes following negative pairing at 20 Hz. ***D***, Intrinsic changes following negative pairing at 5 and 10 Hz. ***E***, Intrinsic changes following negative pairing at 20 Hz. ***F***, Summary of synaptic changes as a function of frequency. ***G***, Summary of intrinsic changes as a function of frequency.

the brain (Milman et al., 2006; Larsson et al., 2020), reduced O-LM excitability (rheobase in control, 33.7 ± 3.2 pA, $n = 8$; rheobase in ARA-S, 50.0 ± 5.7 pA, $n = 8$; Wilcoxon test, $p < 0.05$; Fig. 10*B*). In all cases, this reduced excitability was associated with a reduction of the input resistance tested with subthreshold depolarizing pulses (JZL-184, from 560.9 ± 52.44 MΩ to 417.3 ± 46.1 MΩ, $n = 8$; Wilcoxon test, $p < 0.005$; Fig. 10*C*; ARA-S, from 545 ± 47.2 MΩ to 406 ± 62.55 MΩ, $n = 8$; Fig. 10*D*; Wilcoxon test, $p < 0.05$), indicating that this reduced excitability is mediated by M-type current.

No change in rheobase was observed after negative pairing performed in the presence of JZL-184 or ARA-S (rheobase in

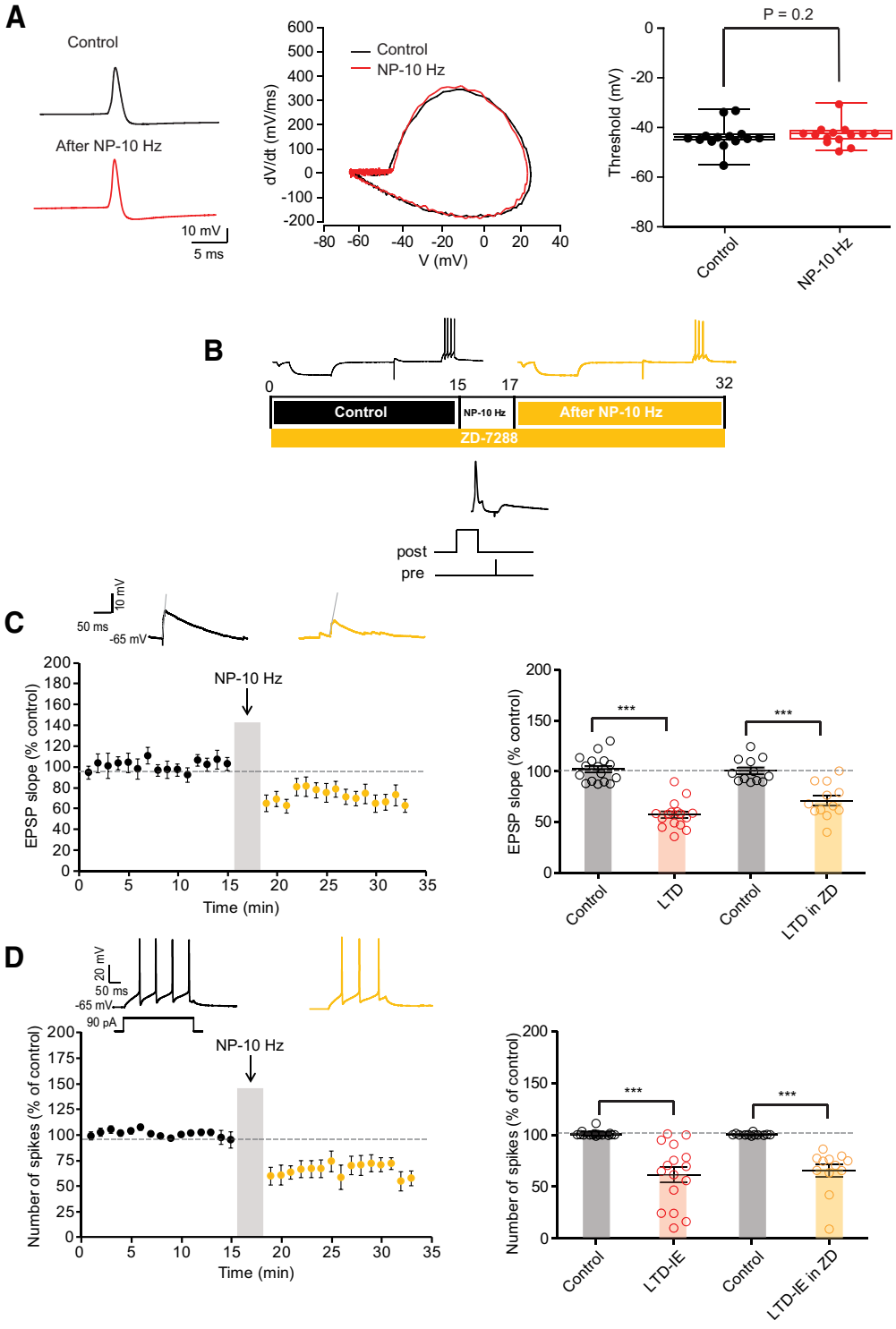

Figure 5. LTD-IE expression, unchanged AP threshold and no incidence of HCN inhibition. ***A***, O-LM AP threshold remains stable following induction of LTD-IE. Left, spike before (black) and after (red) negative pairing. Middle, Phase plots of the spike. Right, Pooled data. ***B***, Experimental protocol for induction of LTD and LTD-IE in the presence of 1 μM ZD-7288. ***C***, Synaptic changes induced by negative pairing in the presence of ZD-7288. Left, Time course. Right, Comparison with control condition. ***D***, Intrinsic changes following negative pairing in the presence of ZD-7288. Left, Time course. Right, Comparison with control condition.

JZL-184, 47.5 ± 5.2 pA, n = 7; rheobase in JZL-184 after NP, 50.0 ± 4.7 pA, n = 7; Wilcoxon, $p > 0.05$; Fig. 10*E*; rheobase in ARA-S, 50.0 ± 5.7 pA, n = 8; rheobase in ARA-S after NP, 53.8 ± 5.9 pA, n = 8; Wilcoxon, $p > 0.05$; Fig. 10*F*), indicating that eCBs not only account for induction of LTD but also for expression of LTD-IE in O-LM interneurons.

Molecular interaction of eCBs with Kv7.2/3 channels

To confirm the direct molecular interaction of eCBs with Kv7.2/3 channels, we first used a modeling approach. For this, we used a model of rat Kv7.2 channel composed of four subunits. Viewed above the membrane, the channel shows its typical homotetramer topology, with the pore located at the center of the

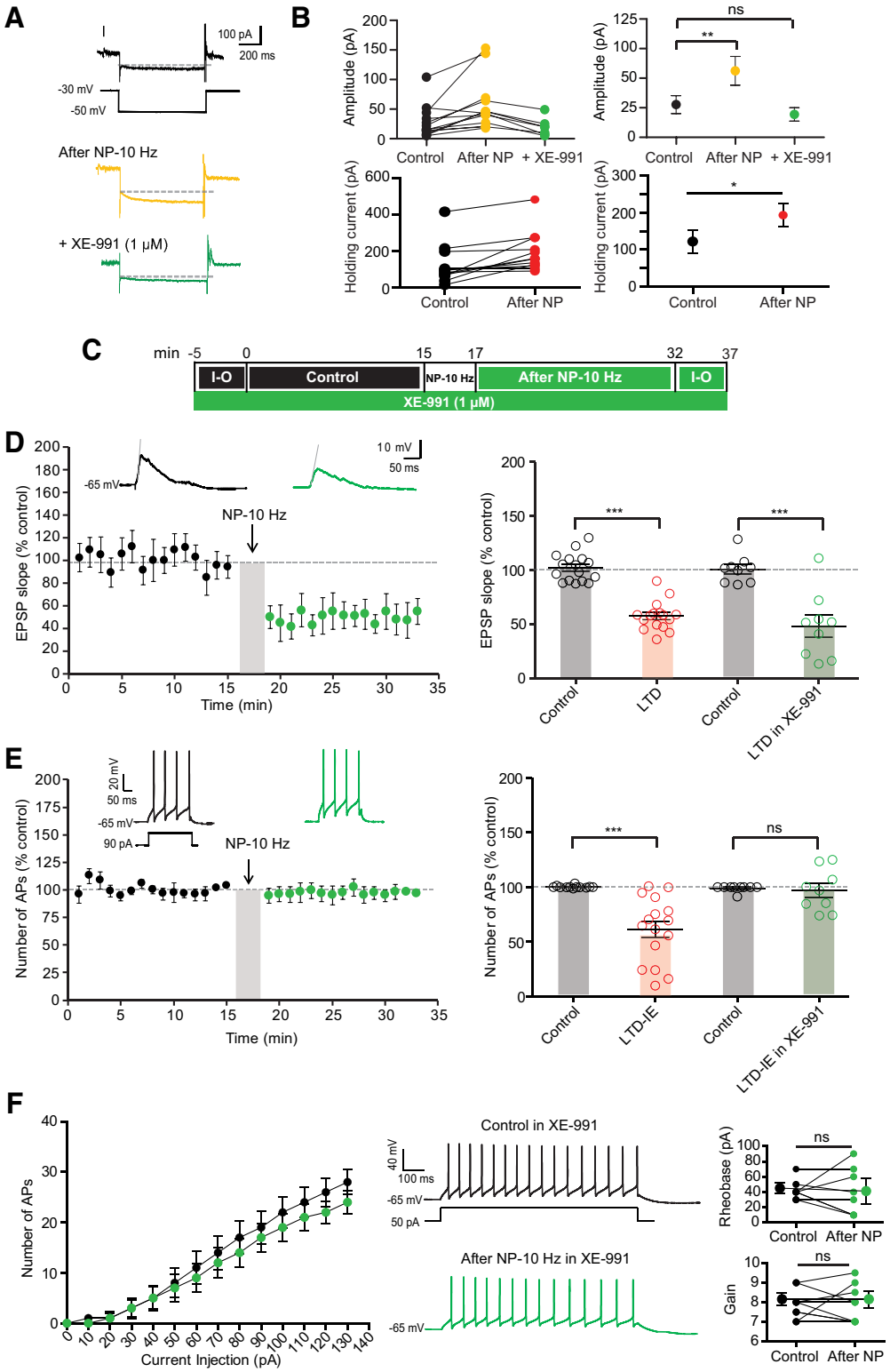

Figure 6. Upregulation of Kv7 channel-mediated current is involved in LTD-IE expression. ***A***, Upregulation of M-type current following induction of LTD-IE. O-LM interneurons are recorded in voltage clamp, and the relaxing component of the M-type current is measured in the presence of HCN channel blocker ZD-7288 (1 μM) before (black) and after (yellow) negative pairing, and in the presence of XE-991 (green). ***B***, Pooled data of the M-current deactivation (top) and holding current at −30 mV. ***C***, Experimental protocol for LTD and LTD-IE induction in the presence of the Kv7 antagonist XE-991 (1 μM). ***D***, LTD is induced in the presence of XE-991. ***E***, LTD-IE is totally absent in the presence of XE-991. ***F***, Input-output curves showing the lack of change in both rheobase and gain.

structure (Fig. 11*A*). The docking of 2-AG on the 3D structure of rat Kv7.2 in the apo state reveals a high affinity binding site for 2-AG located at the junction of subunits B and C in the outer leaflet of the plasma membrane (Fig. 11*A*,*B*). This 2-AG binding site is ideally located to affect the conformational state of the channel. Given the tetrameric structure of the Kv7.2 channel, three other molecules of 2-AG could bind simultaneously to the channel in a symmetric manner, giving a 2-AG stoichiometry of

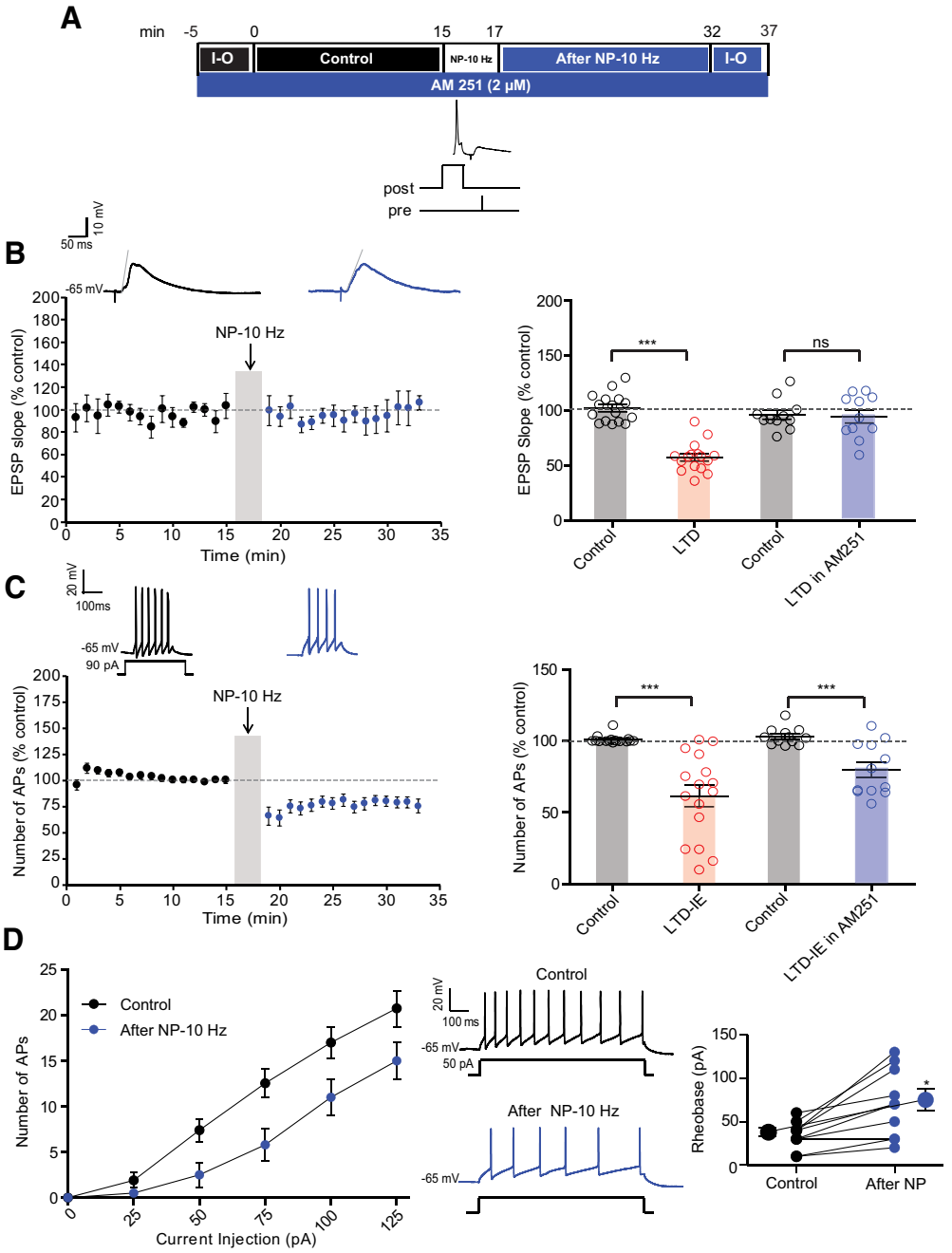

Figure 7. Inhibition of CB1 receptor blocks LTD but not LTD-IE. ***A***, Experimental protocol for induction of LTD and LTD-IE in the presence of 2 μM AM-251. ***B***, Synaptic changes induced by negative pairing in the presence of AM-251. Left, Time course showing a lack of LTD. Right, Comparison with control condition. ***C***, Intrinsic changes following negative pairing in the presence of AM-251. Left, Time course. Right, Comparison with control condition. ***D***, Input-output curves obtained in control and following negative pairing in the presence of AM-251. Left, Curves. Middle, Discharge before and after negative pairing. Right, Analysis of rheobase.

four molecules per Kv7.2 channel, and 2-AG showed a curved shape that fits well with the binding pocket at the junction of subunits B and C (Fig. 11*B*). This binding site consists of a gutter formed by amino acid residues 198–209 in chain B and 245–252 in chain C (Table 1; Fig. 11*C*). To assess whether this gutter could be functionally reconstituted in an acellular system, we used synthetic peptides encompassing each wall of the binding site prepared as monolayers at the air–water interface. The interaction of 2-AG with this reconstituted binding site was studied by microtensiometry (Fig. 11*D*,*E*). When injected in the aqueous subphase underneath the peptide monolayers, 2-AG induced a dramatic surface pressure increase, which indicates a physical interaction between the endocannabinoid and its peptide partners. Interestingly, 2-AG recognized each individual Kv7.2 peptide but also a combination of both peptides, which better mimics the endocannabinoid binding site (Fig. 11*E*). These experimental data confirmed *in silico* simulations.

ARA-S is a structural analog of 2-AG and binds to Kv7 (Larsson et al., 2020). The model shows that ARA-S and 2-AG share the same the binding pocket (Fig. 12*A–C*). The superposition of 2-AG and ARA-S further demonstrates that both eCBs share the same binding site (Fig. 12*C*). Although both eCBs have a high affinity for Kv7.2, the energy of interaction is higher for ARA-S compared with 2-AG (53.6 vs 36.8 kJ.mol^{-1}; Table 1). This difference is essentially because of the negatively charged carboxylate in the polar head group of ARA-S that forms an

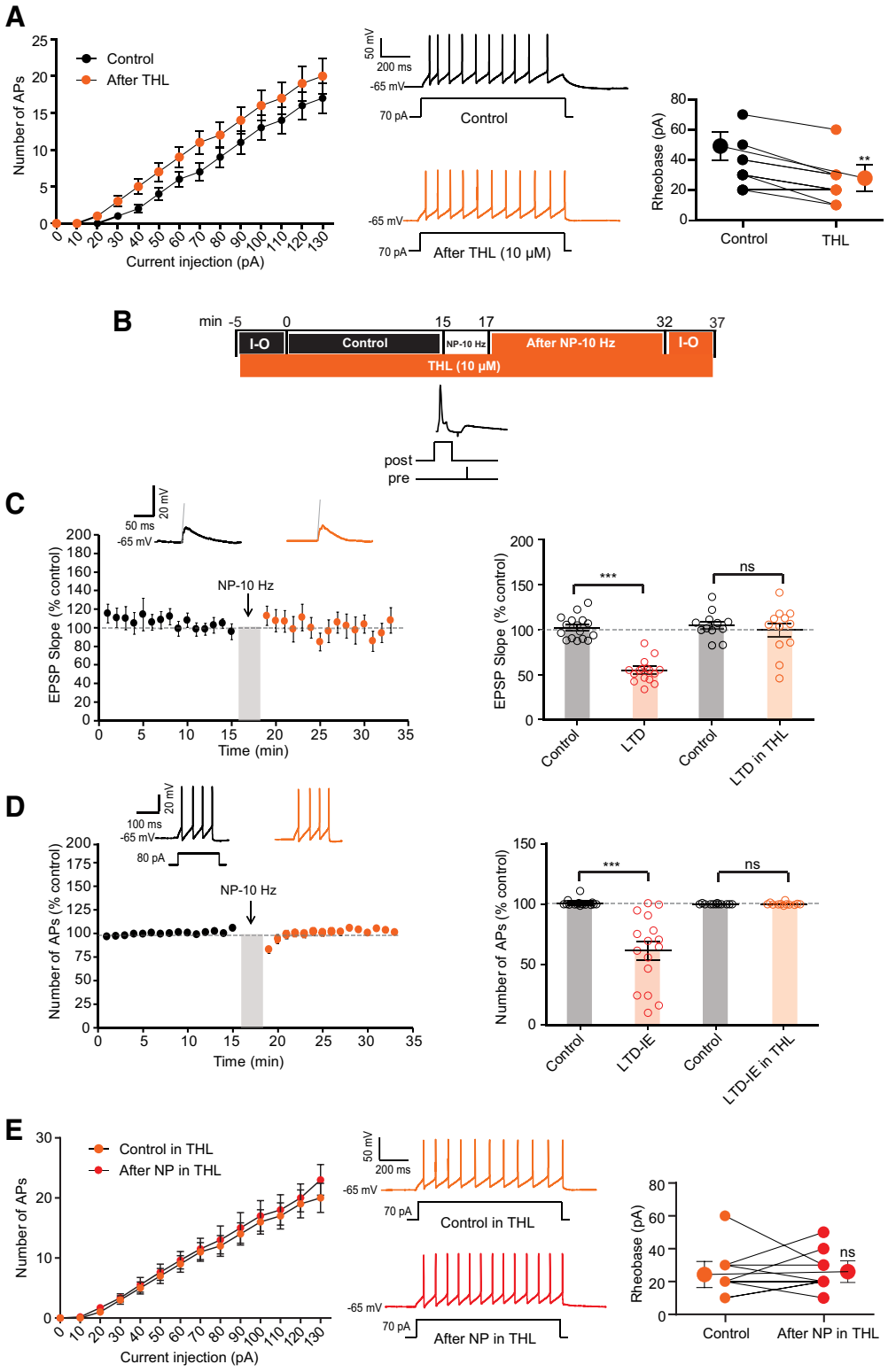

Figure 8. Inhibiting synthesis of 2-AG prevents both LTD and LTD-IE induction. ***A***, Bath application of THL (10 μM) elevates excitability and reduces the rheobase. Left, Input-output curves. Middle, Discharge before and after application of THL. Right, Analysis of rheobase. Wilcoxon test, $^{**}p < 0.01$. ***B***, Experimental protocol for induction of LTD and LTD-IE in the presence of the inhibitor of 2-AG synthesis, THL (10 μM). ***C***, In the presence of THL, no LTD is induced. ***D***, Lack of LTD-IE induction in the presence of THL. ***E***, Input-output curves showing the lack of change in excitability and rheobase. Left, Input-output curves. Middle, Discharge before and after application of THL. Right, Analysis of rheobase.

electrostatic bond with the cationic group of Arg-198 and to the van der Waals contact with Leu-206, which is closer to ARA-S than to 2-AG. Both eCBs adopt the same typical curved structure that fits with the binding site. It is interesting to note that the eCB binding site is highly conserved in Kv7.2 and Kv7.3. The amino acid sequence of the binding motif in chain B (198–209) is identical for both channels, RSLRFLQILRMI.

The presence of a CARC motif within the eCB binding domain suggests that cholesterol could also bind to Kv7.2. Docking

studies confirmed this hypothesis (Fig. 12*D*). The same amino acid residues that interact with 2-AG (i.e., Arg-198, Phe-202, and Leu-206; Fig. 12*D*) are also involved in cholesterol recognition (Fig. 12*D*). Interestingly, when 2-AG was docked onto the Kv7.2 conformer preconstrained by cholesterol, the binding of the eCB was improved, because of the reorientation of aromatic rings (residues Phe-202 and Phe-248), and an optimized geometry of the side chain of Arg-198 (Fig. 12*D*). Overall, the energy of interaction of 2-AG was raised from −36.8 to −53.5 kJ.mol^{-1} (Table 2). Thus, although our data suggest that eCBs can bind to Kv7.2 in a cholesterol-independent mechanism, it is likely that cholesterol could further improve the binding of 2-AG by a conformational selection process. The higher flexibility of 2-AG compared with the sterol, together with the higher energy of interaction of the Kv7.2 complex (Table 2) is compatible with a displacement of cholesterol by 2-AG, leading to the formation of a stable, long-lasting eCB-Kv7.2 complex. To study this possibility, we analyzed the effect of further minimization steps to follow the evolution of the Kv7.2–2-AG complex. Interestingly, we observed that after the initial binding step, 2-AG is gradually attracted deeper in the channel structure as the result of a typical induced fit mechanism (Fig. 12*E*). At the end of this process, the energy of interaction was further increased to reach −81.4 kJ.mol^{-1}, which represents a gain of +52%. Thus, our *in silico* data support the notion of a long-lasting eCB-Kv7.2 complex. We conclude that this eCB-Kv7 complex may account for the reduced excitability found in O-LM interneurons.

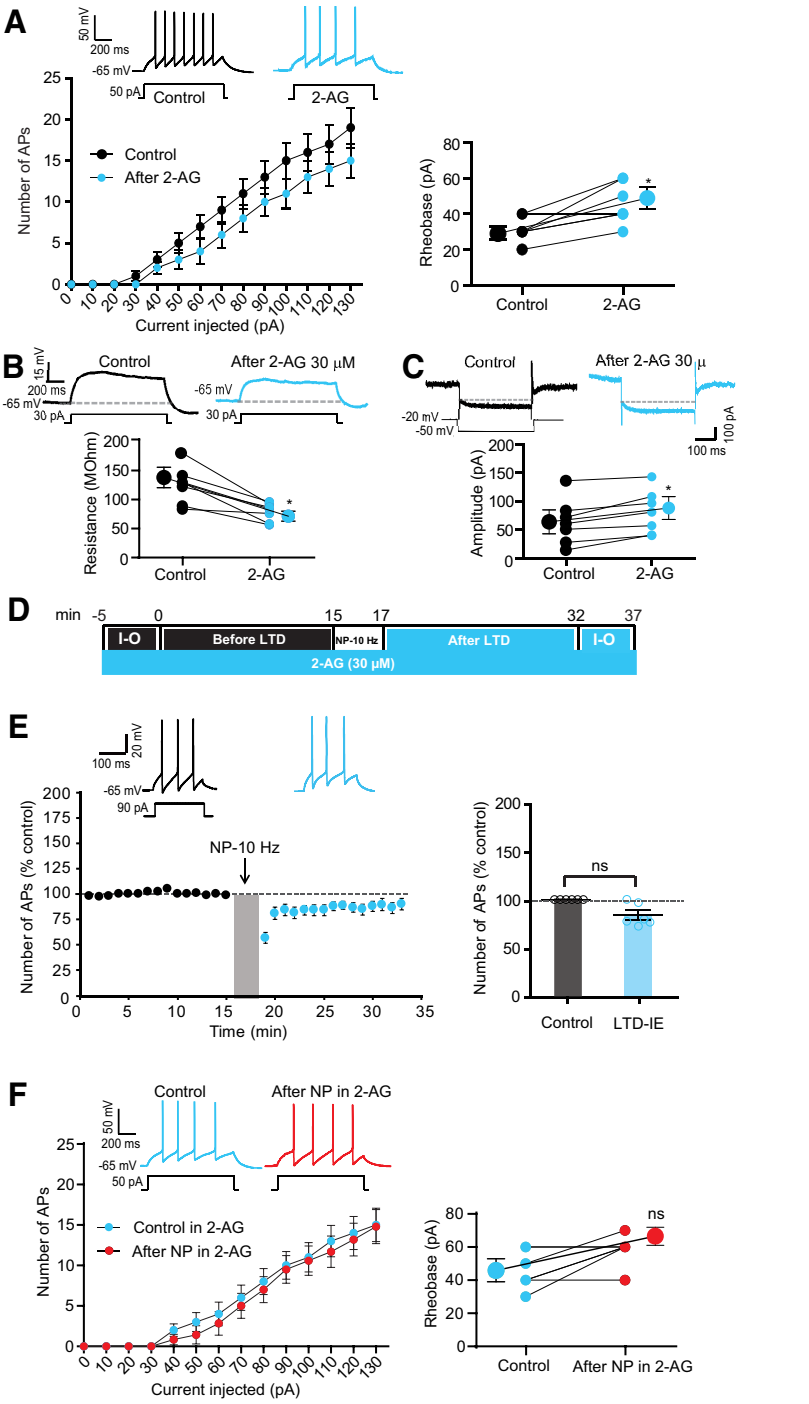

Figure 9. Application of 2-AG mimics and occludes LTD-IE. ***A***, Bath application of 2-AG (30 μM) reduces intrinsic excitability and elevates the rheobase in O-LM interneurons. Left, Input-output curves and discharge before and after application of 2-AG. Right, Analysis of rheobase. Wilcoxon test, $^*p < 0.05$. ***B***, 2-AG reduces input resistance tested with depolarizing subthreshold current pulses. Left, Representative traces. Right, Pooled data. Wilcoxon test, $^*p < 0.05$. ***C***, Sample traces and pooled data showing upregulation of M-type current following 20 min of 2-AG (30 μM) application. O-LM interneurons are recorded in voltage clamp, and the relaxing component is measured in the presence of HCN channel blocker ZD-7288 (1 μM) before (black) and after (light blue) 2-AG. Wilcoxon test, $^*p < 0.05$. ***D***, Experimental protocol for induction of LTD-IE in the presence of 2-AG. ***E***, 2-AG occludes induction of LTD-IE. Left, Time course. Right, Pooled data. ***F***, Input-output curves showing the lack of change in excitability and rheobase. Left, Input-output curves and discharge before and after negative pairing in the presence of 2-AG. Right, Analysis of rheobase.

Discussion

Our study reveals that O-LM interneurons unexpectedly express intrinsic plasticity in parallel to synaptic plasticity. In fact, we show here that negative correlation between presynaptic and postsynaptic activity in the theta range induces long-lasting depression of both synaptic transmission and intrinsic neuronal excitability. These two modifications are synergistic and provide a certain level of functional redundancy because both types of plasticity tend to reduce the excitation of O-LM interneurons. Mechanistically, our study indicates that both LTD and LTD-IE in O-LM interneurons depend on the biosynthesis of eCBs that target (1) presynaptic CB1 receptors to regulate release of glutamate and (2) postsynaptic Kv7 channels present in the dendrites of O-LM interneurons to regulate intrinsic excitability. This mechanism of LTD-IE can potentially have very important consequences in the feedback loop that O-LM interneurons establish with CA1 pyramidal neurons in the local hippocampal circuit.

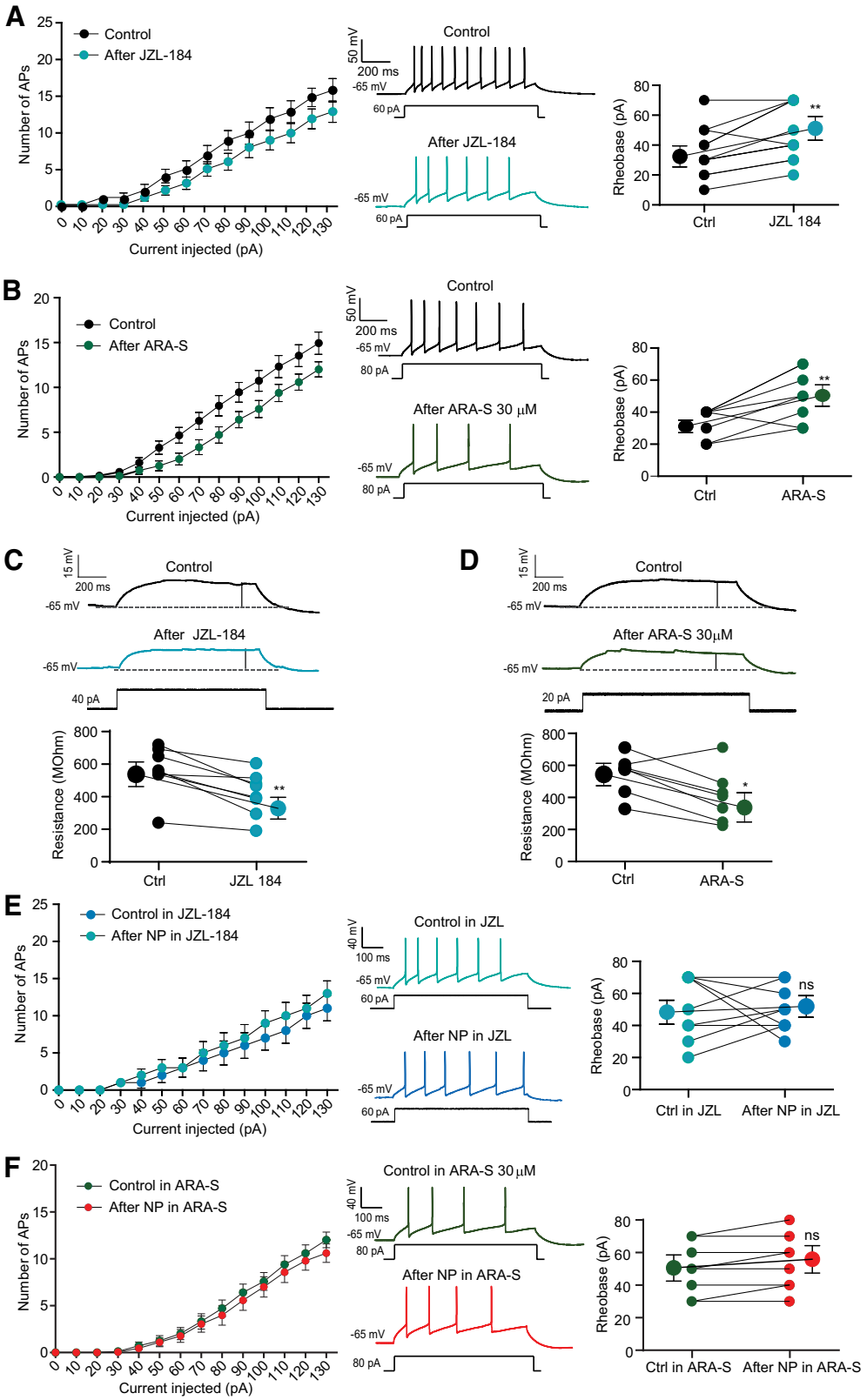

Figure 10. Effects of endocannabinoids on O-LM excitability. ***A***, The 2-AG degradation inhibitor, JZL-184 (1 μM), reduces intrinsic excitability in O-LM interneurons. Left, Input-output curves. Middle, Discharge before and after application of JZL-184. Right, Analysis of rheobase. Wilcoxon test, $^{**}p < 0.01$. ***B***, ARA-S (1 μM) reduces O-LM excitability. Left, Input-output curves. Middle, Discharge before and after application of ARA-S. Right, Analysis of rheobase. Wilcoxon test, $^{**}p < 0.01$. ***C***, JZL-184 reduces input resistance tested with subthreshold depolarizing pulses. Top, Representative traces. Bottom, pooled data. Wilcoxon test, $^{**}p < 0.01$. ***D***, ARA-S reduces input resistance tested with subthreshold depolarizing pulses. Top, Representative traces. Bottom, Pooled data. Wilcoxon test, $^{**}p < 0.01$. ***E***, Lack of intrinsic plasticity in the presence of JZL-184. Left, Input-output curves. Middle, Discharge before and after application of JZL-184. Right, Analysis of rheobase. ***F***, Lack of intrinsic plasticity in the presence of ARAI-S. Left, Input-output curves. Middle, Discharge before and after application of ARA-S. Right, Analysis of the rheobase.

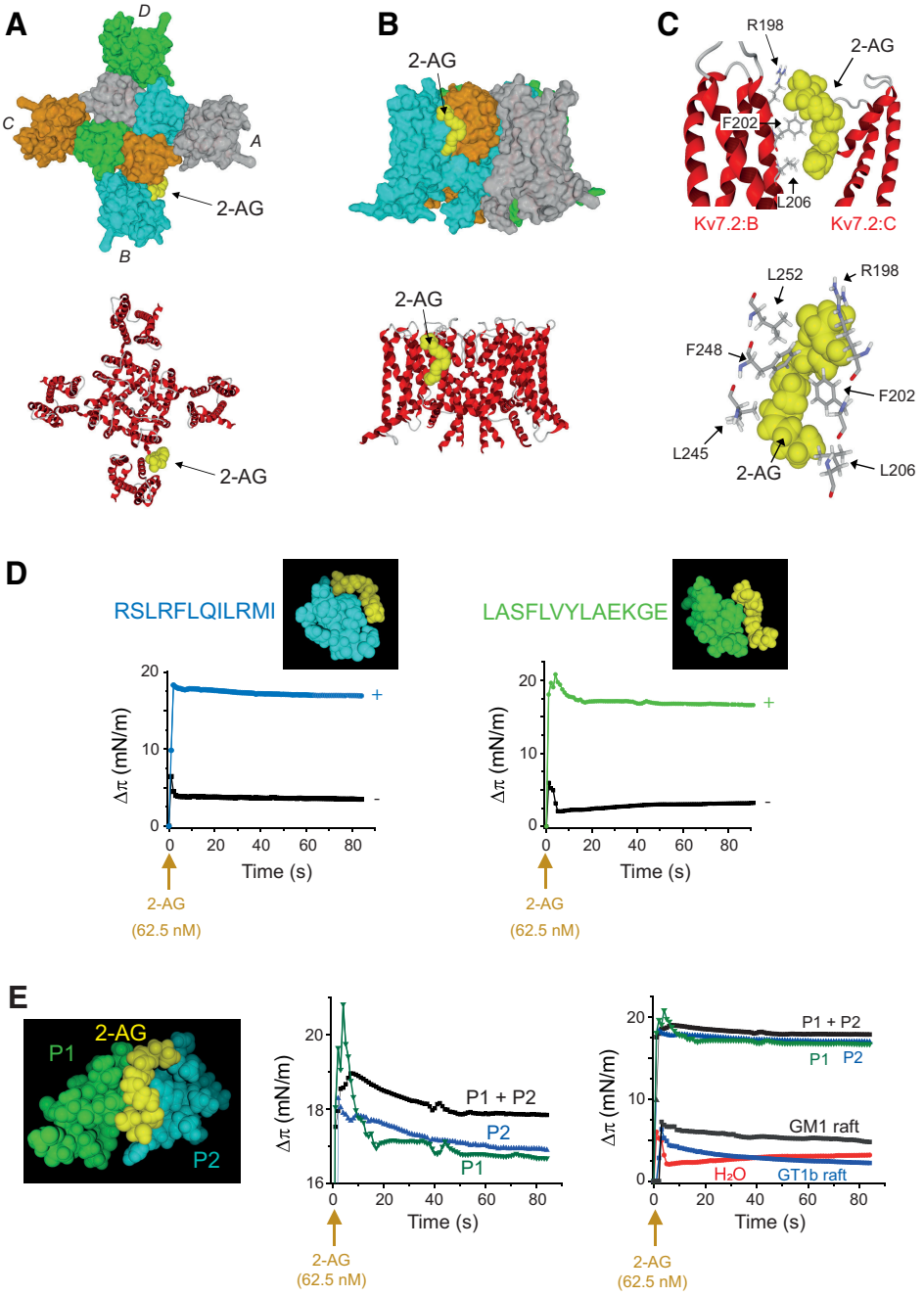

Figure 11. Docking and binding of 2-AG on Kv7.2 in the apo state. ***A***, Kv7.2 consists of a homotetramer of four subunits (A, B, C, D, respectively, colored in gray, cyan, orange, and green area on left). The pore (still closed in the apo state) is located at the center of the structure. The 2-AG binding site is located in the outer leaflet of the plasma membrane at the junction on chains B and C. The secondary structure of the channel is shown on the right. ***B***, Lateral views of the Kv7.2 channel showing the 2-AG binding site. The surface view on the left illustrates the involvement of both chains B (cyan) and C (orange) in the binding site. ***C***, The 2-AG in the endocannabinoid binding pocket formed by subunits B and C of Kv7.2. Contacts with key amino acid residues of the CARC domain (Arg-198, Phe-202, and Leu-206 in subunit B) are clearly shown (left). Right, Amino acid residues of subunits B (Arg-198, Phe-202, and Leu-206) and C (Leu-245, Phe-248, and Leu-252) in close contact with 2-AG. For clarity only the key triad of amino acids in each subunit is shown. ***D***, Molecular modeling of 2-AG (yellow) in complex with the KV7.2 regions encompassing peptides RSLRFLQILRMI (cyan) and LASFLVYLAEKGE (green). When these synthetic peptides were reconstituted at monolayers at the air–water interface, the addition of 2-AG (62.5 nM) resulted in a marked increase in the surface pressure, which demonstrates a physical interaction between the peptides and the endocannabinoid (+, cyan and green curves). At this concentration, 2-AG injected in water in absence of the peptide monolayers (−, black curves) had a very limited effect on the surface pressure. The data show a typical experiment representative of three distinct studies. ***E***, Molecular modeling of 2-AG (yellow) in complex with the Kv7.2 regions encompassing peptides P1 (LASFLVYLAEKGE) in green and P2 (RSLRFLQILRMI) in cyan. When P1 and P2 synthetic peptides were reconstituted in monolayers at the air–water interface, the addition of 2-AG (62.5 nM) resulted in a marked increase in the surface pressure, which demonstrates a physical interaction between the peptides and the endocannabinoid. In all cases, 2-G induced a biphasic response consisting of a dramatic increase followed a relaxation (left). Note that the best response is obtained with a combination of P1 and P2. Control experiments without peptides (H_2O) or with ganglioside monolayers (GM1 and GT1b reconstituted rafts) showed that 2-AG interacts selectively with P1 and P2 (right). The data show a typical experiment representative of three distinct studies.

Table 1. Energy of interaction (in kJ.mol^{-1}) of each amino acid residue of Kv7.2 involved in 2-AG and ARA-S binding

Amino acid	2-AG	ARA-S
Arg-198 (chain B)	−6.0	−13.6
Phe-202 (chain B)	−9.4	−9.5
Leu-206 (chain B)	−2.0	−7.9
Ile-209 (chain B)	−1.2	−5.8
Leu-245 (chain C)	−3.5	−1.7
Phe-248 (chain C)	−8.9	−9.8
Leu-249 (chain C)	−1.6	−2.6
Leu-252 (chain C)	−4.2	−2.7
Total	−36.8	−53.6

Table 2. Energy of interaction (in kJ.mol^{-1}) of each amino acid residue of Kv7.2 involved in 2-AG binding in absence of cholesterol or after cholesterol release

Amino acid	2-AG bound without cholesterol	2-AG bound after cholesterol release	Cholesterol bound
Arg-198 (chain B)	−6.0	−14.9	−13.1
Ser-199(chain B)	0	−2.8	−3.1
Phe-202 (chain B)	−9.4	−20.0	−22.6
Leu-206 (chain B)	−2.0	−2.5	−2.4
Ile-209 (chain B)	−1.2	−1.4	−0.8
Leu-245 (chain C)	−3.5	−2.0	0
Phe-248 (chain C)	−8.9	−7.7	−7.7
Leu-249 (chain C)	−1.6	0	0
Leu-252 (chain C)	−4.2	−2.2	0
Total	−36.8	−53.5	−49.7

For comparison, the energy of interaction of cholesterol bound to Kv7.2 is also given.

Functional synergy between synaptic and intrinsic modifications

Long-lasting synaptic plasticity is generally associated with synergistic regulation of intrinsic neuronal excitability (Debanne et al., 2019). For instance, in hippocampal pyramidal neurons, both LTP and LTD are respectively induced in parallel with EPSP-Spike (E-S) potentiation and E-S depression (Daoudal et al., 2002; Campanac and Debanne, 2008). In fast-spiking PV interneurons, both LTP and LTP-IE are induced by high-frequency stimulation of glutamatergic inputs (Campanac et al., 2013). The present study shows that this rule is also verified in O-LM interneurons as LTD and LTD-IE occur in parallel. Interestingly, a positive correlation was found between LTD and LTD-IE values. In addition, presynaptic or postsynaptic activation alone was found to be unable to induce both LTD and LTD-IE, suggesting that induction of both LTD and LTD-IE are mechanistically linked. Furthermore, induction of both LTD and LTD-IE in O-LM interneurons was highly sensitive to the frequency of stimulation. In fact, as previously established for LTD in mouse O-LM interneurons (Péterfi et al., 2012), the optimal frequency was found within the theta range (10 Hz). This suggests that eCB release could be optimal at this specific frequency.

Our study points to the conclusion that eCBs play a critical role in induction of both LTD and LTD-IE in O-LM interneurons. First, inhibition of CB1 receptor with AM-251 prevented LTD induction. Second, inhibition of DAG lipase by THL totally abolished both LTD and LTD-IE induction. Third, application of eCBs as 2-AG or ARA-S reduced intrinsic excitability in O-LM interneurons.

Intrinsic plasticity in GABAergic interneurons

Activity-dependent plasticity has been reported in only a few type of cortical interneurons including perisomatic inhibitory interneurons such as PV baskets cells (Campanac et al., 2013; Gainey et al., 2018) or GABAergic interneuron-targeting neurogliaform interneurons (Chittajallu et al., 2020). Regarding SOM interneurons, only one study has reported intrinsic excitability following learning (McKay et al., 2013). However, this study is not entirely conclusive as it was based on comparison of different interneurons from different animals. It was not known so far whether single O-LM interneurons expressed intrinsic plasticity. Our study fills this gap. O-LM interneurons thus represent the third class of GABAergic interneurons showing plasticity of intrinsic neuronal excitability, suggesting that plasticity of inhibitory circuits is not only mediated by synaptic plasticity but that intrinsic changes take a large part in this regulation. In all three interneuron types, intrinsic plasticity involves the regulation of the following Kv channels: Kv1.1 for PV basket cells (Campanac et al., 2013), Kv4 for neurogliaform interneurons (Chittajallu et al., 2020), and Kv7 for O-LM cells (the present study). However, although the two other plasticity mechanisms involve a loss of Kv function, the present plasticity reveals a gain of Kv function.

Involvement of Kv7 channels in intrinsic plasticity

We show here that Kv7 channels represent the main ion channel by which neuronal excitability in O-LM interneurons is regulated. The M-current was found to be of greater amplitude after negative pairing and after 2-AG application. In addition, input resistance tested with depolarizing pulse was decreased after 2-AG application. Furthermore, LTD-IE expression (but not LTD) was prevented in the presence of the selective antagonist of Kv7 channels, XE-991. Although Kv7 channels have been suspected to be involved in functional plasticity (Baculis et al., 2020), our study provides the first direct evidence for its involvement in activity-dependent regulation of intrinsic excitability.

In contrast to most neurons, the dendrites of O-LM interneurons contain a high density of Nav channels that makes possible AP initiation in the dendrites (Martina et al., 2000). Therefore, Kv7 channels located in the dendrites (Lawrence et al., 2006) may critically control O-LM excitability. Kv7 channels are also present in CA3 basket cells and in bistratified interneurons (Fidzinski et al., 2015). Interestingly, PV basket interneurons express cannabinoid-dependent LTD (Péterfi et al., 2012), suggesting that cannabinoid-dependent LTD-IE could be induced in these interneurons.

Diacylglycerol (DAG) lipase and Kv7 channels are both located on O-LM proximal dendrites as well in the somatic region (Lawrence et al., 2006; Péterfi et al., 2012), thus strongly suggesting that 2-AG produced in the dendrites will be able to modulate nearby Kv7 channels.

eCB signaling in O-LM interneurons

eCBs (especially 2-AG) have emerged as very important retrograde messengers throughout the brain. eCBs are involved in many brain functions including regulation of presynaptic transmitter release underlying learning and memory (Castillo et al., 2012), neurologic disorders (Cristino et al., 2020) and psychiatric disorders (Lutz et al., 2015). Interneurons function is also controlled by eCB. O-LM interneurons express high levels of the DAG lipase-α in perisynaptic regions around excitatory inputs (Katona et al., 2006; Yoshida et al., 2006). In addition, a specific eCB-dependent presynaptic LTD that requires mGluR1 activation and postsynaptic calcium elevation for its induction has been described in O-LM cells (Péterfi et al., 2012).

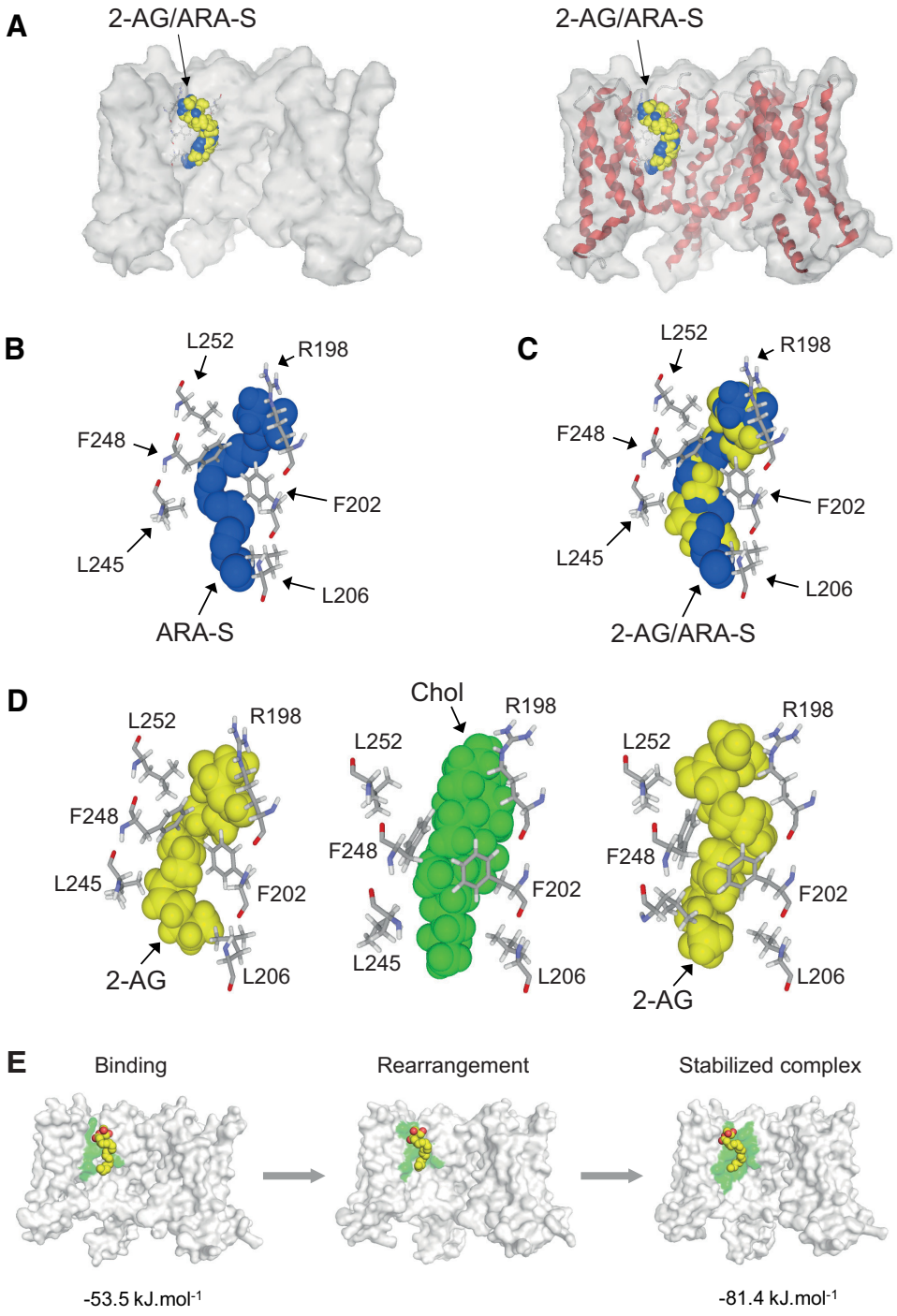

Figure 12. Binding of 2-AG and ARA-S to Kv7.2. ***A***, Superposition of 2-AG (yellow) and ARA-S (blue) bound to Kv7.2 in surface view (left) and secondary structure/surface rendition (right). Both endocannabinoids occupy a similar volume and bind to the same site. ***B***, Amino acid residues of Kv7.2 in close contact with ARA-S. ***C***, Superposition of 2-AG and ARA-S in the cannabinoid binding pocket of Kv7.2. ***D***, Previous docking of cholesterol enhances interaction of 2-AG for Kv7.2. Left, Docking of 2-AG (yellow) on Kv7.2. Middle, Docking of cholesterol (green) on Kv7.2 reorients the aromatic rings of Phe-202 and Phe-258 and rearranges the side chain of Arg-198. Right, Docking of 2-AG (yellow) on the cholesterol-optimized conformation of Kv7.2 shown in the middle. Note the reorientation of Leu-245, which does not interact with cholesterol (middle). The aromatic rings of Phe-202 and Phe-248 have retained the specific orientations imposed by cholesterol. ***E***, *In silico* simulations of the evolution of the 2-AG-Kv7.2 complex. 2-AG is colored in yellow with oxygen atoms in red. The Kv7-2 surface is in light gray. The fingerprint created by the amino acid residues involved in 2-AG binding is colored in green. After the initial binding step (left), both the Kv7.2 channel and the endocannabinoid undergo a mutual conformational rearrangement (center) leading to a stabilized complex (right) with a high interaction energy.

Our results show that 2-AG or ARA-S application reduces intrinsic excitability of O-LM interneurons. In fact, both compounds elevate the rheobase and partially occlude induction of LTD-IE. A study indicated that ARA-S facilitates activation of the M-current mediated by Kv7.2/3 in an *in vitro* expression system (Larsson et al., 2020). In fact, ARA-S hyperpolarizes the activation curve by 20 mV and increases by a factor of two the conductance of the M- current. However, in that study, no indication about a potential persistent effect of ARA-S was identified, nor any significant effect of 2-AG on Kv7 channels was reported,

suggesting that an additional factor present in O-LM interneurons but absent in oocytes allows Kv7 regulation by 2-AG. Nevertheless, our molecular modeling, confirmed by an *in vitro* reconstitution of a functional endocannabinoid binding site, indicates that 2-AG or ARA-S bind to Kv7.2 at the junction between two adjacent subunits with a very high affinity, suggesting a persistent binding and possibly a persistent activation of these channels. The identified eCB binding site is highly conserved in Kv7.2 and Kv7.3. The amino acid sequence of the binding motif in chain B (198–209) is identical for both channels: 198–**R**SLR**F**LQI**L**RMI–209. This motif is a consensus CARC domain, with the key amino acid residues in boldface. Such CARC motifs in TM domains are recognized by cholesterol (Fantini et al., 2016). Thus, our data suggest the intriguing possibility of a regulatory cholesterol–eCB exchange in Kv7 channels function, in line with previous studies focused on CB1 receptors (Di Scala et al., 2018). The binding motif in chain C of Kv7.2 has the following amino acid sequence in Kv7.2: 245–LASFLVYL–252, which belongs to an inverted CARC motif (Fantini et al., 2016) that encompasses residues 245–255 (**L**ASFLV**Y**LAE**K**; key residues in boldface). This motif is also conserved in Kv7.3 (**L**SSFLV**Y**LVE**K**; key residues in boldface). Together, these data further strengthen the hypothesis of a dual cholesterol-eCB regulation of Kv7.2 and Kv7.3 function.

Our data indicate that the regulation of Kv7 channels by eCBs is not mediated by CB1 receptor but rather eCBs may directly interact with Kv7 channels. First, inhibiting CB1 receptors with AM-251 blocked induction of LTD but not LTD-IE. Furthermore, molecular modeling indicates that 2-AG is able to directly bind to Kv7.2/3 channels, which is confirmed by monolayer experiments with the two peptides.

Lipids as eCBs are known to control the biophysical properties of a wide range of ion channels (Elinder and Liin, 2017), including Kv1 (Decher et al., 2010; Carta et al., 2014), Kv4 (Villarroel and Schwarz, 1996), and HCN (Fogle et al., 2007) channels that are involved in long-term plasticity of intrinsic excitability (Frick et al., 2004; Fan et al., 2005; Campanac et al., 2008, 2013; Gasselin et al., 2017). Thus, our study may lead to open a new line of future investigations.

Functional consequences

The functional consequences of a reduction in O-LM excitability mediated by the upregulation of Kv7 channel-mediated M-type current may be multiple. At the cellular level, upregulation of M-type current may enhance intrinsic resonance in O-LM cells in the depolarizing range. In fact, both Kv7 and HCN channels are known to be responsible for intrinsic resonance at two specific voltage levels in CA1 pyramidal neurons (Hu et al., 2002). O-LM interneurons possess these two channels and also display intrinsic resonance (Gastrein et al., 2011). At the local circuit level, a reduced excitability of O-LM interneurons may reduce inhibition at distal dendrites of CA1 pyramidal neurons and thus favor induction of LTP at temporoammonic pathway (Leão et al., 2012). In parallel, the reduced inhibition of stratum radiatum interneurons may consequently reduce LTP induction at Schaffer collateral pathway (Leão et al., 2012). This switch can potentially have an important role for the acquisition of new spatial memories, and alteration could result in pathologic consequences. Furthermore, the eCB-dependent dampening of O-LM excitability may represent a way to limit excitation during excessive network excitation. Further studies will be required to circumvent the functional consequence of LTD-IE in O-LM interneurons.

References

Alle H, Jonas P, Geiger JR (2001) PTP and LTP at a hippocampal mossy fiber-interneuron synapse. Proc Natl Acad Sci U S A 98:14708–14713.

Baculis BC, Zhang J, Chung HJ (2020) The role of Kv7 channels in neural plasticity and behavior. Front Physiol 11:568667.

Campanac E, Daoudal G, Ankri N, Debanne D (2008) Downregulation of dendritic I(h) in CA1 pyramidal neurons after LTP. J Neurosci 28:8635–8643.

Campanac E, Debanne D (2008) Spike timing-dependent plasticity: a learning rule for dendritic integration in rat CA1 pyramidal neurons. J Physiol 586:779–793.

Campanac E, Gasselin C, Baude A, Rama S, Ankri N, Debanne D (2013) Enhanced intrinsic excitability in basket cells maintains excitatory-inhibitory balance in hippocampal circuits. Neuron 77:712–722.

Carta M, Lanore F, Rebola N, Szabo Z, Da Silva SV, Lourenço J, Verraes A, Nadler A, Schultz C, Blanchet C, Mulle C (2014) Membrane lipids tune synaptic transmission by direct modulation of presynaptic potassium channels. Neuron 81:787–799.

Castillo PE, Younts TJ, Chávez AE, Hashimotodani Y (2012) Endocannabinoid signaling and synaptic function. Neuron 76:70–81.

Chittajallu R, Auville K, Mahadevan V, Lai M, Hunt S, Calvigioni D, Pelkey KA, Zaghloul KA, McBain CJ (2020) Activity-dependent tuning of intrinsic excitability in mouse and human neurogliaform cells. Elife 9:e57571.

Cristino L, Bisogno T, Di Marzo V (2020) Cannabinoids and the expanded endocannabinoid system in neurological disorders. Nat Rev Neurol 16:9–29.

Daoudal G, Hanada Y, Debanne D (2002) Bidirectional plasticity of excitatory postsynaptic potential (EPSP)-spike coupling in CA1 hippocampal pyramidal neurons. Proc Natl Acad Sci U S A 99:14512–14517.

Debanne D, Inglebert Y, Russier M (2019) Plasticity of intrinsic neuronal excitability. Curr Opin Neurobiol 54:73–82.

Decher N, Streit AK, Rapedius M, Netter MF, Marzian S, Ehling P, Schlichthörl G, Craan T, Renigunta V, Köhler A, Dodel RC, Navarro-Polanco RA, Preisig-Müller R, Klebe G, Budde T, Baukrowitz T, Daut J (2010) RNA editing modulates the binding of drugs and highly unsaturated fatty acids to the open pore of Kv potassium channels. EMBO J 29:2101–2113.

Delmas P, Brown DA (2005) Pathways modulating neural KCNQ/M (Kv7) potassium channels. Nat Rev Neurosci 6:850–862.

Di Scala C, Fantini J, Yahi N, Barrantes F, Chahinian H (2018) Anandamide revisited: how cholesterol and ceramides control receptor-dependent and receptor-independent signal transmission pathways of a lipid neurotransmitter. Biomolecules 8:31.

Elinder F, Liin SI (2017) Actions and mechanisms of polyunsaturated fatty acids on voltage-gated ion channels. Front Physiol 8:43.

Fan Y, Fricker D, Brager DH, Chen X, Lu H-C, Chitwood RA, Johnston D (2005) Activity-dependent decrease of excitability in rat hippocampal neurons through increases in I(h). Nat Neurosci 8:1542–1551.

Fantini J, Di Scala C, Evans LS, Williamson PTF, Barrantes FJ (2016) A mirror code for protein-cholesterol interactions in the two leaflets of biological membranes. Sci Rep 6:21907.

Fidzinski P, Korotkova T, Heidenreich M, Maier N, Schuetze S, Kobler O, Zuschratter W, Schmitz D, Ponomarenko A, Jentsch TJ (2015) KCNQ5 K(+) channels control hippocampal synaptic inhibition and fast network oscillations. Nat Commun 6:6254.

Flores A, Ramirez-Franco J, Desplantes R, Debreux K, Ferracci G, Wernert F, Blanchard M-P, Maulet Y, Youssouf F, Sangiardi M, Iborra C, Popoff MR, Seagar M, Fantini J, Lévêque C, El Far O (2019) Gangliosides interact with synaptotagmin to form the high-affinity receptor complex for botulinum neurotoxin B. Proc Natl Acad Sci U S A 116:18098–18108.

Fogle KJ, Lyashchenko AK, Turbendian HK, Tibbs GR (2007) HCN pacemaker channel activation is controlled by acidic lipids downstream of diacylglycerol kinase and phospholipase A2. J Neurosci 27:2802–2814.

Frick A, Magee J, Johnston D (2004) LTP is accompanied by an enhanced local excitability of pyramidal neuron dendrites. Nat Neurosci 7:126–135.

Gainey MA, Aman JW, Feldman DE (2018) Rapid disinhibition by adjustment of PV intrinsic excitability during whisker map plasticity in mouse S1. J Neurosci 38:4749–4761.

Gasselin C, Inglebert Y, Ankri N, Debanne D (2017) Plasticity of intrinsic excitability during LTD is mediated by bidirectional changes in h-channel activity. Sci Rep 7:14418.

Gastrein P, Campanac E, Gasselin C, Cudmore RH, Bialowas A, Carlier E, Fronzaroli-Molinieres L, Ankri N, Debanne D (2011) The role of hyperpolarization-activated cationic current in spike-time precision and intrinsic resonance in cortical neurons *in vitro*. J Physiol 589:3753–3773.

Hu H, Vervaeke K, Storm JF (2002) Two forms of electrical resonance at theta frequencies, generated by M-current, h-current and persistent Na+ current in rat hippocampal pyramidal cells. J Physiol 545:783–805.

Katona I, Urbán GM, Wallace M, Ledent C, Jung K-M, Piomelli D, Mackie K, Freund TF (2006) Molecular composition of the endocannabinoid system at glutamatergic synapses. J Neurosci 26:5628–5637.

Klausberger T, Magill PJ, Márton LF, Roberts JDB, Cobden PM, Buzsáki G, Somogyi P (2003) Brain-state- and cell-type-specific firing of hippocampal interneurons *in vivo*. Nature 421:844–848.

Klausberger T, Somogyi P (2008) Neuronal diversity and temporal dynamics: the unity of hippocampal circuit operations. Science 321:53–57.

Kuba H, Yamada R, Ishiguro G, Adachi R (2015) Redistribution of Kv1 and Kv7 enhances neuronal excitability during structural axon initial segment plasticity. Nat Commun 6:8815.

Kullmann DM, Lamsa KP (2007) Long-term synaptic plasticity in hippocampal interneurons. Nat Rev Neurosci 8:687–699.

Kullmann DM, Moreau AW, Bakiri Y, Nicholson E (2012) Plasticity of inhibition. Neuron 75:951–962.

Lamsa KP, Heeroma JH, Somogyi P, Rusakov DA, Kullmann DM (2007) Anti-Hebbian long-term potentiation in the hippocampal feedback inhibitory circuit. Science 315:1262–1266.

Larsson JE, Karlsson U, Wu X, Liin SI (2020) Combining endocannabinoids with retigabine for enhanced M-channel effect and improved KV7 subtype selectivity. J Gen Physiol 152:e202012576.

Lawrence JJ, Saraga F, Churchill JF, Statland JM, Travis KE, Skinner FK, McBain CJ (2006) Somatodendritic Kv7/KCNQ/M channels control interspike interval in hippocampal interneurons. J Neurosci 26:12325–12338.

Leão RN, Mikulovic S, Leão KE, Munguba H, Gezelius H, Enjin A, Patra K, Eriksson A, Loew LM, Tort ABL, Kullander K (2012) OLM interneurons differentially modulate CA3 and entorhinal inputs to hippocampal CA1 neurons. Nat Neurosci 15:1524–1530.

Li X, Zhang Q, Guo P, Fu J, Mei L, Lv D, Wang J, Lai D, Ye S, Yang H, Guo J (2021) Molecular basis for ligand activation of the human KCNQ2 channel. Cell Res 31:52–61.

Lutz B, Marsicano G, Maldonado R, Hillard CJ (2015) The endocannabinoid system in guarding against fear, anxiety and stress. Nat Rev Neurosci 16:705–718.

Martina M, Vida I, Jonas P (2000) Distal initiation and active propagation of action potentials in interneuron dendrites. Science 287:295–300.

McKay BM, Oh MM, Disterhoft JF (2013) Learning increases intrinsic excitability of hippocampal interneurons. J Neurosci 33:5499–5506.

McMahon LL, Kauer JA (1997) Hippocampal interneurons express a novel form of synaptic plasticity. Neuron 18:295–305.

Milman G, Maor Y, Abu-Lafi S, Horowitz M, Gallily R, Batkai S, Mo F-M, Offertaler L, Pacher P, Kunos G, Mechoulam R (2006) N-arachidonoyl L-serine, an endocannabinoid-like brain constituent with vasodilatory properties. Proc Natl Acad Sci U S A 103:2428–2433.

Pangalos M, Donoso JR, Winterer J, Zivkovic AR, Kempter R, Maier N, Schmitz D (2013) Recruitment of oriens-lacunosum-moleculare interneurons during hippocampal ripples. Proc Natl Acad Sci U S A 110:4398–4403.

Pelkey KA, Chittajallu R, Craig MT, Tricoire L, Wester JC, McBain CJ (2017) Hippocampal GABAergic Inhibitory Interneurons. Physiol Rev 97:1619–1747.

Pelletier JG, Lacaille J-C (2008) Long-term synaptic plasticity in hippocampal feedback inhibitory networks. Prog Brain Res 169:241–250.

Perez Y, Morin F, Lacaille JC (2001) A Hebbian form of long-term potentiation dependent on mGluR1a in hippocampal inhibitory interneurons. Proc Natl Acad Sci U S A 98:9401–9406.

Péterfi Z, Urbán GM, Papp OI, Németh B, Monyer H, Szabó G, Erdélyi F, Mackie K, Freund TF, Hájos N, Katona I (2012) Endocannabinoid-mediated long-term depression of afferent excitatory synapses in hippocampal pyramidal cells and GABAergic interneurons. J Neurosci 32:14448–14463.

Shah MM, Migliore M, Valencia I, Cooper EC, Brown DA (2008) Functional significance of axonal Kv7 channels in hippocampal pyramidal neurons. Proc Natl Acad Sci U S A 105:7869–7874.

Titley HK, Brunel N, Hansel C (2017) Toward a neurocentric view of learning. Neuron 95:19–32.

Udakis M, Pedrosa V, Chamberlain SEL, Clopath C, Mellor JR (2020) Interneuron-specific plasticity at parvalbumin and somatostatin inhibitory synapses onto CA1 pyramidal neurons shapes hippocampal output. Nat Commun 11:4395.

Varga C, Golshani P, Soltesz I (2012) Frequency-invariant temporal ordering of interneuronal discharges during hippocampal oscillations in awake mice. Proc Natl Acad Sci U S A 109:E2726–2734.

Vasuta C, Artinian J, Laplante I, Hébert-Seropian S, Elayoubi K, Lacaille J-C (2015) Metaplastic regulation of CA1 Schaffer collateral pathway plasticity by Hebbian MGluR1a-mediated plasticity at excitatory synapses onto somatostatin-expressing interneurons. eNeuro 2:ENEURO.0051-15.2015.

Vickers ED, Clark C, Osypenko D, Fratzl A, Kochubey O, Bettler B, Schneggenburger R (2018) Parvalbumin-interneuron output synapses show spike-timing-dependent plasticity that contributes to auditory map remodeling. Neuron 99:720–735.e6.

Villarroel A, Schwarz TL (1996) Inhibition of the Kv4 (Shal) family of transient K+ currents by arachidonic acid. J Neurosci 16:1016–1025.

Yoshida T, Fukaya M, Uchigashima M, Miura E, Kamiya H, Kano M, Watanabe M (2006) Localization of diacylglycerol lipase-alpha around postsynaptic spine suggests close proximity between production site of an endocannabinoid, 2-arachidonoyl-glycerol, and presynaptic cannabinoid CB1 receptor. J Neurosci 26:4740–4751.